PAPER

Check for updates

cis-Tetrachlorido-bis(indazole)osmium(IV) and its osmium(III) analogues: paving the way towards the *cis*-isomer of the ruthenium anticancer drugs KP1019 and/or NKP1339†‡

Gabriel E. Büchel, [ID] a,b Susanne Kossatz,b Ahmad Sadique,b Peter Rapta,*c Michal Zalibera, [ID] c Lukas Bucinsky,c Stanislav Komorovsky, [ID] d Joshua Telser, [ID] *e Jörg Eppinger, [ID] a Thomas Reinerb,f and Vladimir B. Arion [ID] *g

The relationship between *cis–trans* isomerism and anticancer activity has been mainly addressed for square-planar metal complexes, in particular, for platinum(II), *e.g.*, *cis*- and *trans*-[PtCl$_2$(NH$_3$)$_2$], and a number of related compounds, of which, however, only *cis*-counterparts are in clinical use today. For octahedral metal complexes, this effect of geometrical isomerism on anticancer activity has not been investigated systematically, mainly because the relevant isomers are still unavailable. An example of such an octahedral complex is *trans*-[RuCl$_4$(Hind)$_2$]$^-$, which is in clinical trials now as its indazolium (KP1019) or sodium salt (NKP1339), but the corresponding *cis*-isomers remain inaccessible. We report the synthesis of Na[*cis*-Os^{III}Cl$_4$(κN2-1*H*-ind)$_2$]·(Na[**1**]) suggesting a route to the *cis*-isomer of NKP1339. The procedure involves heating (H$_2$ind)[Os^{IV}Cl$_5$(κN1-2*H*-ind)] in a high boiling point organic solvent resulting in an Anderson rearrangement with the formation of *cis*-[Os^{IV}Cl$_4$(κN2-1*H*-ind)$_2$] ([**1**]) in high yield. The transformation is accompanied by an indazole coordination mode switch from κN1 to κN2 and stabilization of the 1*H*-indazole tautomer. Fully reversible spectroelectrochemical reduction of [**1**] in acetonitrile at 0.46 V *vs.* NHE is accompanied by a change in electronic absorption bands indicating the formation of *cis*-[Os^{III}Cl$_4$(κN2-1*H*-ind)$_2$]$^-$ ([**1**]$^-$). Chemical reduction of [**1**] in methanol with NaBH$_4$ followed by addition of *n*Bu$_4$NCl afforded the osmium(III) complex *n*Bu$_4$N[*cis*-Os^{III}Cl$_4$(κN2-1*H*-ind)$_2$] (*n*Bu$_4$N[**1**]). A metathesis reaction of *n*Bu$_4$N[**1**] with an ion exchange resin led to the isolation of the water-soluble salt Na[**1**]. The X-ray diffraction crystal structure of [**1**]·Me$_2$CO was determined and compared with that of *trans*-[Os^{IV}Cl$_4$(κN2-1*H*-ind)$_2$]·2Me$_2$SO (**2**·2Me$_2$SO), also prepared in this work. EPR spectroscopy was performed on the Os^{III} complexes and the results were analyzed by ligand-field and quantum chemical theories. We furthermore assayed effects of [**1**] and Na[**1**] on cell viability and proliferation in comparison with *trans*-[Os^{IV}Cl$_4$(κN1-2*H*-ind)$_2$] [**3**] and cisplatin and found a strong reduction of cell viability at concentrations between 30 and 300 μM in different cancer cell lines (HT29, H446, 4T1 and HEK293). HT-29 cells are less sensitive to cisplatin than 4T1 cells, but more sensitive to [**1**] and Na[**1**], as shown by decreased proliferation and viability as well as an increased late apoptotic/necrotic cell population.
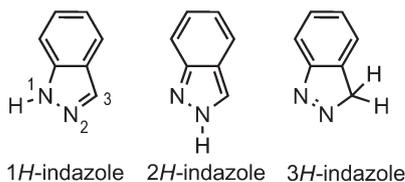
*a*Division of Physical Sciences and Engineering, KAUST Catalysis Center, King Abdullah University of Science and Technology, Thuwal 23955-6900, Saudi Arabia
*b*Department of Radiology, Memorial Sloan Kettering Cancer Center, 1275 York Avenue, New York, New York 10065, USA
*c*Slovak University of Technology, Institute of Physical Chemistry and Chemical Physics, Radlinského 9, 81237 Bratislava, Slovakia. E-mail: peter.rapta@stuba.sk
*d*Institute of Inorganic Chemistry, Slovak Academy of Sciences, Dúbravská cesta 9, SK-84536 Bratislava, Slovakia
*e*Department of Biological, Chemical and Physical Sciences, Roosevelt University, 430 S. Michigan Avenue, Chicago, Illinois 60605, USA. E-mail: jtelser@roosevelt.edu
*f*Department of Radiology, Weill Cornell Medical College, New York, NY 10065, USA

*g*University of Vienna, Faculty of Chemistry, Institute of Inorganic Chemistry, Währinger Str. 42, A-1090 Vienna, Austria. E-mail: vladimir.arion@univie.ac.at
†Dedicated to Professor Dr Karl Wieghardt on the occasion of his 75th birthday anniversary.
‡Electronic supplementary information (ESI) available: Atom numbering scheme for NMR resonance assignment (Fig. S1), details of crystal structures of [**1**]·Me$_2$CO and [**2**]·2Me$_2$SO (Fig. S2 and S3), the ^{1}H NMR spectrum of [**1**] (Fig. S4), details of UV-vis-NIR spectroelectrochemistry and UV-vis spectra of [**1**] and *n*Bu$_4$N[**1**] in Me$_2$SO and acetonitrile (Fig. S5–S9), the Q-band EPR spectrum of Na[**1**] in aqueous solution (Fig. S10), the powder X-band EPR spectrum of *n*Bu$_4$N[**1**] (Fig. S11), the results of Alamar Blue assay (Table S1). CCDC 1544885 and 1544886. For ESI and crystallographic data in CIF or other electronic format see DOI: 10.1039/c7dt02194a

Introduction

Indazole derivatives are characterized by a variety of applications as anti-inflammatory, antimicrobial, antihypertensive, antiprotozoal, antiobesity, and antifungal agents.[1–3] They have been found to be active as inhibitors of nitric oxide synthase (NOS),[4] bacterial gyrases,[5] hydrolases,[6] and various kinases.[7–9] The ruthenium(III) complexes H$_2$ind[*trans*-RuCl$_4$(κN2-1*H*-indazole)$_2$] (KP1019) and Na[*trans*-RuCl$_4$(κN2-1*H*-indazole)$_2$] (NKP1339) are in clinical trials as potential anticancer agents.[10] Indazole, usually referred to as 1*H*-indazole, exists in three tautomeric forms (Chart 1). 1*H*-Indazole is the dominant tautomer in the gas phase and aqueous solution,[11,12] as well as in metal complexes, however, some substituted organic 2*H*-indazoles are known[13] as well as rare, inorganic examples such as an organoruthenium(II) complex with 2-methyl-indazole,[14] and the osmium(IV) complexes *trans*-[Os^{IV}Cl$_4$(κN1-2*H*-ind)$_2$],[15] and (H$_2$ind)[Os^{IV}Cl$_5$(κN1-2*H*-ind)].[16] The synthesis of the latter complex along with (H$_2$ind)[Os^{IV}Cl$_5$(κN2-1*H*-ind)] made an estimation of the effect of indazole tautomer identity on the antiproliferative activity of osmium(IV) complexes in different human cancer cell lines possible.

After the discovery of the antiproliferative activity of cisplatin in 1965,[17] the *cis*-geometry was long believed to be a prerequisite for the anticancer activity of metal compounds.[18,19] Even though this situation changed over the years as several *trans*-isomers were synthesized and discovered to exhibit higher antiproliferative potency than their *cis*-congeners,[20] with some of them having the advantage of not showing cross resistance to cisplatin,[21] there are no *trans*-isomers in clinical use today. However, all these examples are dealing with square-planar metal complexes. The importance of the *cis*–*trans* isomerism in octahedral coordination complexes has been known since Alfred Werner's time.[22] In the case of octahedral ruthenium and osmium compounds, some cases of isomeric pairs are well-documented for azole heterocycles[23,24] and bis-picolinamide ruthenium(III) dihalide complexes.[25] The structurally related osmium(III) pyridine derivatives, *cis*- and *trans*-[OsCl$_4$(Py)$_2$]$^-$ are also known, and both were crystallographically characterized.[26] Overall, the number of cytotoxic Werner's type osmium complexes is increasing.[27] However, elucidation of structure–activity relationship remains an important task for the understanding of the mode of action of such complexes and the development of more effective anticancer agents than those exploited today.

Following our interest in investigation of the chemistry of osmium(IV)–indazole-tautomer interconversion, we studied the isomerization mechanism of *n*Bu$_4$N[Os^{IV}Cl$_5$(κN1-2*H*-ind)] into *n*Bu$_4$N[Os^{IV}Cl$_5$(κN2-1*H*-ind)] and the results will be reported in due course. In addition, it was found that prolonged heating of (H$_2$ind)[Os^{IV}Cl$_5$(κN1-2*H*-ind)] in the high boiling point solvent 1,1,2,2-tetrachloroethane afforded an unprecedented product of *cis*-configuration, namely *cis*-[Os^{IV}Cl$_4$(κN2-1*H*-ind)$_2$] ([**1**]).

The present study of [**1**] adds to the growing family of osmium(IV) and osmium(III) azole compounds.[28] The complexes presented in this work are stable in aqueous and/or Me$_2$SO solution for at least 24 h (osmium(III) compounds in the absence of air oxygen). Upon one-electron reduction of the metal center the tautomer coordinated to metal remains intact as also reported for *trans*-[Os^{III}Cl$_4$(κN1-2*H*-ind)$_2$]$^-$.[29] Quite recently, a pH dependent indazole tautomerization has been reported, wherein the stabilization of one of the tautomers was achieved by coordination of an indazole-pendant azamacrocyclic scorpiand to Cu^{II} or Zn^{II}.[30]

Herein, we describe the synthesis of *cis*-[Os^{IV}Cl$_4$(κN2-1*H*-ind)$_2$] ([**1**]) and its one electron reduced species (*n*Bu$_4$N)[**1**] and Na[**1**] (Chart 2). These complexes are spectroscopically characterized, in particular by electron paramagnetic resonance (EPR), a technique which has been shown to be very useful in unravelling the solution structure of Ru^{III} anti-cancer drug candidates,[31] as well as other Ru^{III} complexes.[32] EPR has been less widely applied to Os^{III} complexes of any type because of the paucity of such compounds and frequently their inherently more challenging experimental EPR properties.[33,34] In addition, the antiproliferative activity of the two octahedral *cis*-isomers [**1**] and Na[**1**], along with the X-ray diffraction structures of *cis*- and *trans*-[Os^{IV}Cl$_4$(κN2-1*H*-ind)$_2$] ([**1**] and [**2**], respectively) are reported. This discovery offers the pathway to *cis*-isomers of investigational anticancer drugs KP1019 and NKP1339 and a subsequent opportunity to investigate structure–activity relationships for octahedral *cis*/*trans*-[RuCl$_4$(κN2-1*H*-ind)$_2$]$^-$ isomers.
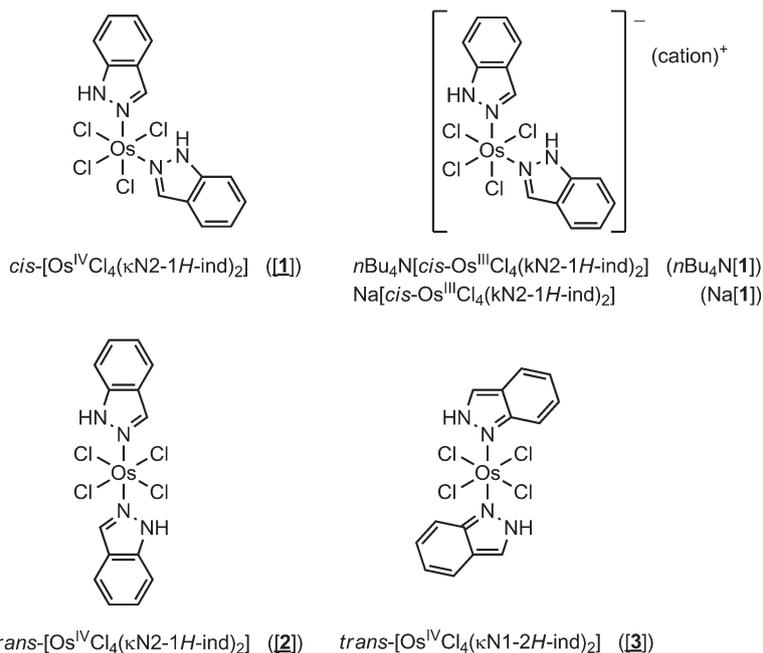
Experimental section

Materials

OsO$_4$ (99.8%) was purchased from Johnson-Matthey, while *n*Bu$_4$NBr, NaBH$_4$, 1*H*-indazole, KBr and Dowex Marathon C-resin Na$^+$ form were from Sigma-Aldrich. All chemicals were used without further purification.

Synthesis of osmium complexes

The starting compounds (H$_2$ind)[OsCl$_6$] and (H$_2$ind)[OsCl$_5$(κN1-2*H*-ind)] were prepared according to the literature protocols.[16,35]

cis-[OsCl$_4$(κN2-1*H*-ind)$_2$]·Me$_2$CO ([1]·Me$_2$CO). (H$_2$ind)[OsCl$_5$(κN1-2*H*-ind)] (160 mg, 0.26 mmol) was stirred in 1,1,2,2-tetrachloroethane (30 ml) at 128 °C for 10 h. Removal of the solvent at reduced pressure, washing the residue with diethyl ether and drying *in vacuo* afforded a black solid of [**1**]. Yield: 140 mg, 93%. Elemental analysis was performed on a sample crystallized from Me$_2$CO. Calcd for C$_{14}$H$_{12}$Cl$_4$N$_4$Os·Me$_2$CO (M_r = 626.39), %: C, 32.60; H, 2.90; N,

Chart 1 The tautomers of indazole with five-membered ring atom numbering given on the left tautomer.

Chart 2 Compounds reported in this work. Underlined numbers indicate compounds studied by single crystal X-ray diffraction. Complex [3] relevant to this work was reported previously.[15]

8.94; O, 2.55. Found, %: C, 32.83; H, 2.89; N, 8.88; O, 2.57. Analytical data for **1**: HRMS (positive) in MeOH: m/z 532.9713 $[OsCl_3(Hind)_2]^+$; calcd m/z 532.9652. ESI-MS in MeOH (negative): m/z 567 $[Os^{IV}Cl_4(Hind)_2-H]^-$. MIR, cm^{-1}: 641, 747, 784, 800, 964, 1000, 1079, 1239, 1360, 1467, 1515, 1627, 2928, and 3314. UV–vis (Me$_2$CO), λ_{max}, nm (ε, M^{-1} cm^{-1}): 371 (1632), 406 (1704), 582 (410), 729 (130). UV–vis (acetonitrile), λ_{max}, nm (ε, M^{-1} cm^{-1}): 228 (2663), 268 (2660), 364 (1663), 405 (1635), 510 sh, 613 (508), 726 (116). UV–vis (chloroform), λ_{max}, nm (ε, M^{-1} cm^{-1}): 243 (1228), 271 (1413), 286 sh, 365 (740), 409 (853), 559 (220), 725 (82). UV–vis (DMF), λ_{max}, nm (ε, M^{-1} cm^{-1}): 286 (2686), 369 (1727), 400 (1636), 507 (683), 614 (530), 726 (175). UV–vis (Me$_2$SO), λ_{max}, nm (ε, M^{-1} cm^{-1}): 273 (2900), 285 (2865), 364 (1533), 407 (1600), 618 (521), 724 (137). UV–vis (ethanol), λ_{max}, nm (ε, M^{-1} cm^{-1}): 370 (1665), 402 (1663), 562 (376), 608 sh, 725 (96). UV–vis (THF), λ_{max}, nm (ε, M^{-1} cm^{-1}): 296 (2423), 374 (1677), 400 (1797), 543 (364), 726 (83). ^{1}H NMR (Me$_2$SO-d_6, 500.26 MHz), δ: −9.42 (s, 2H, H$_3$), 1.35 (t, J = 7.96 Hz, 2H, H$_6$), 4.66 (d, J = 8.98 Hz, 2H, H$_4$), 8.04 (t, J = 8.06 Hz, 2H, H$_7$), 10.87 (d, 2H, H$_5$, J = 8.23 Hz), 16.49 (s, 2H, H$_3$) ppm. ^{13}C{^{1}H} NMR (Me$_2$SO-d_6, 125.82 MHz), δ: 69.29 (C$_8$ or C$_9$), 69.97 (C$_8$ or C$_9$), 74.78 (C$_5$), 101.66 (C$_7$), 143.40 (C$_4$), 177.94 (C$_6$), 189.05 (C$_3$) ppm. Suitable crystals for the X-ray diffraction study were grown by slow evaporation of a solution of [**1**] in Me$_2$CO. For atom numbering and assignment of NMR resonances see Fig. S1 in ESI.‡

(nBu$_4$N)[cis-Os^{III}Cl$_4$(κN2-1H-ind)$_2$] (nBu$_4$N[1]). To a solution of cis-[Os^{IV}Cl$_4$(κN2-1H-ind)$_2$] (30 mg, 0.04 mmol) in methanol (1 ml) under nitrogen NaBH$_4$ (3 mg, 0.079 mmol) was added. After stirring for 1 h nBu$_4$NCl (16 mg) in water (1 ml) was added. The orange solution produced a yellow-brown precipitate, which

was filtered, washed with cold water and diethyl ether and dried *in vacuo* to give a light-brown solid. Yield: 24 mg, 61%. Analytical data for nBu$_4$N[**1**]: ESI-MS in MeOH (negative): m/z 567 $[Os^{III}Cl_4(Hind)_2]^-$, 332 $[Os^{III}Cl_4]^-$. MIR, cm^{-1}: 656, 752, 785, 833, 959, 1002, 1081, 1243, 1355, 1440, 1482, 1506, 1625, 2827, 2960 and 3285. ^{1}H NMR (CD$_3$OD, 500.26 MHz), δ: −22.16 (br. s, 2H), −7.06 (br. s, 2H), −0.63 (br. s, 2H), 0.32 (br. s, 2H), 1.12 (t, 12H, J = 7.5 Hz), 1.34 (br. s, 2H), 1.55 (sxt, 8H, J = 7.4 Hz), 1.96 (qui, 8H, J = 6.9 Hz), 2.33 (br. s, 2H), 3.55 (t, 8H, J = 7.8 Hz) ppm.

Na[cis-Os^{III}Cl$_4$(κN2-1H-ind)$_2$]·H$_2$O (Na[1]·H$_2$O). Compound nBu$_4$N[**1**] (50 mg, 0.06 mmol) was dissolved in a 1 : 1 mixture of methanol and water (50 ml) under a nitrogen atmosphere. Ion exchanger Dowex Marathon C Na$^+$-form was added to the solution after soaking for 12 h in water. After stirring the suspension for 5 min the ion exchange resin was separated by filtration and the solution lyophilized to give a light-brown solid. Yield: 23 mg, 62%. Calcd for C$_{14}$H$_{12}$Cl$_4$N$_4$NaOs·H$_2$O (M_r = 609.32), %: C, 27.60; H, 2.32; N, 9.20. Found, %: C, 28.08; H, 2.15; N, 8.72. ESI-MS in MeOH (negative): m/z 567.93 $[Os^{III}Cl_4(Hind)_2]^-$. MIR, cm^{-1}: 652, 749, 834, 964, 1002, 1080, 1241, 1356, 1438, 1471, 1510, 1627, 2817 and 3313, 3510. ^{1}H NMR (MeOH-d$_4$, 500.26 MHz): δ −22.16 (br. s, 2H), −7.06 (br. s, 2H), −0.63 (br. s, 2H), 0.32 (br. s, 2H), 1.34 (br. s, 2H), 2.33 (br. s, 2H) ppm.

$trans$-[OsCl$_4$(κN2-1H-ind)$_2$]·2Me$_2$SO ([2]·2Me$_2$SO). (H$_2$ind)$_2$[Os^{IV}Cl$_6$] (166 mg, 0.25 mmol) was heated in the solid state at 150 °C in a glass oven for 45 h. The black product was extracted with methanol in a Soxhlet extractor for 24 h. The solvent was evaporated to give a blue product $trans$-[OsCl$_4$(κN1-2H-ind)$_2$] [**3**] contaminated with [**2**]. Very slow evaporation of a dimethyl sulfoxide solution of the raw product led to the separation of few red crystals of [**2**]·2Me$_2$SO.

Paper

Physical measurements

UV–vis spectra were recorded on a Jasco V-630 UV–vis spectrophotometer using samples dissolved in Me_2CO, MeCN, DMF, Me_2SO, EtOH, and THF. MIR spectra in the region 4000–600 cm^{-1} were recorded with a Thermo Nicolet NEXUS 470 FT-IR spectrometer (Thermo Fisher Scientific, USA), in KBr pellets. Electrospray ionization mass spectrometry was carried out with a Thermo Scientific LCQ Fleet ion trap instrument (Thermo Scientific, Waltham, MA, USA) by using methanol as a solvent. High-resolution mass spectrometry (HRMS) was performed on a LTQ Orbitrap Velos instrument (Thermo Scientific, Waltham, MA, USA). Expected and measured isotope distributions were compared. The cyclic voltammetric studies were performed in a home-made miniature electrochemical cell using a platinum wire as working and counter electrodes, and a silver wire as a pseudoreference electrode. Ferrocene served as the internal potential standard. The redox potentials in Me_2SO solutions were recalculated *vs.* Standard Hydrogen Electrode (NHE) using the known redox potential of ferrocene (0.64 V) *vs.* NHE. A Heka PG310USB (Lambrecht, Germany) potentiostat with a PotMaster 2.73 software package was used in cyclic voltammetric and spectroelectrochemical studies. *In situ* spectroelectrochemical measurements were performed on a spectrometer Avantes, Model AvaSpec-2048x14-USB2. Halogen and deuterium lamps were used as light sources (Avantes, Model AvaLight-DH-S-BAL) under an argon atmosphere in a spectroelectrochemical cell kit (AKSTCKIT3) with the Pt-microstructured honeycomb working electrode, purchased from Pine Research Instrumentation. The cell was positioned in the CUV-UV Cuvette Holder (Ocean Optics) connected to the diode-array UV-vis-NIR spectrophotometer by optical fibers. UV-vis-NIR spectra were processed using the AvaSoft 7.7 software package. The ^1H and ^{13}C NMR spectra were recorded at 500 and 125 MHz on a Bruker Avance III 500 MHz (Ultrashield Magnet) instrument by using MeOH-d_4 and Me_2SO-d_6 as solvents. The solvent residual peak for ^1H and ^{13}C was used as an internal reference. EPR spectra were recorded using an EMXplus X-band EPR spectrometer (Bruker, Germany) equipped with a high-sensitivity resonator ER 4119 HS and an ER 4141 VT variable temperature unit as well as with a modified Bruker EMX spectrometer equipped with an Oxford Instruments cryostat for liquid helium temperature (10–20 K) X-band spectra and a modified Varian spectrometer for superfluid helium temperature (2 K) Q-band (~35 GHz) spectra. The EPR spectra were analyzed and simulated with the Easyspin toolbox.[36] Ligand-field parameters for LS d^5 systems were calculated using a fitting program originally provided by B. R. McGarvey[33b] and modified by J. Telser.[32]

Crystallographic structure determination

X-ray diffraction measurements of [1]·Me_2CO and [2]·$2Me_2SO$ were performed on a Bruker X8 APEX-II CCD diffractometer at 199 and 100 K, respectively. The data were processed using SAINT software.[37] The structures were solved by direct methods and refined by full-matrix least-squares techniques. Non-hydrogen atoms were refined with anisotropic displacement para-

meters. H atoms were placed at calculated positions and refined as riding atoms in the subsequent least squares model refinements. The isotropic thermal parameters were estimated to be 1.2 times the values of the equivalent isotropic thermal parameters of the non-hydrogen atoms to which hydrogen atoms are bonded. The following computer programs and equipment were used: solution SHELXS-2014 and refinement, SHELXL-2014;[38] molecular diagrams, ORTEP;[39] computer, Pentium IV. Crystal data, data collection parameters, and structure refinement details are given in Table 1. CCDC 1544885 and 1544886 contain the CIFs for this manuscript.

Computational details

The Gaussian09 package[40] has been used for the geometry optimizations of the anion $^2[\mathbf{1}]^-$ (total charge minus one and doublet spin state). The unrestricted B3LYP[41]/def2-TZVP[42] level of theory has been employed and the core electrons of osmium were treated *via* the SDD pseudo potential.[43] Vibrational analysis showed that the optimized geometry of $^2[\mathbf{1}]^-$ is free of imaginary (negative) frequencies.

The *g*-tensor values[44] have been theoretically determined using two different approaches. The first attempt employed the ORCA software package[45] at the DFT (with either BLYP or B3LYP functional) and complete active space self-consistent field (CASSCF) levels of theory. Here the scalar ZORA Hamiltonian[46] and uncontracted double zeta (UDZ) basis sets[47] have been used together with inclusion of solvent effects *via* the conductor-like screening model (COSMO)[48] of Me_2SO. The spin–orbit coupling (SOC) effects have been included as a perturbation (with ORCA input settings: grid 7; soctype 3; socflags 1,3,3,1). The CASSCF calculation used five electrons in five orbitals and has been run as state specific (accounting formally for 10 roots). SOC treatment in CASSCF has been performed under default settings of the relativity module (dosoc

Table 1 Crystal data and details of data collection for [1]·Me_2CO and [2]·$2Me_2SO$

Compound	[1]·Me_2CO	[2]·$2Me_2SO$
Empirical formula	$C_{17}H_{18}Cl_4N_4OOs$	$C_{18}H_{24}Cl_4N_4O_2OsS_2$
F_w	626.35	724.53
Space group	$P2_1/c$	$P2_1/n$
a [Å]	13.1258(4)	10.2354(6)
b [Å]	12.2645(4)	14.3781(6)
c [Å]	17.8016(4)	16.4733(9)
β [°]	131.537(1)	91.046(2)
V [Å³]	2145.07(11)	2423.9(2)
Z	4	4
λ [Å]	1.54184	0.71073
ρ_{calcd} [g cm^{-3}]	1.939	1.985
Crystal size [mm]	0.20 × 0.08 × 0.06	0.10 × 0.10 × 0.02
T [K]	199(2)	100(2)
μ [mm^{-1}]	15.943	5.898
$R_1{}^a$	0.0180	0.0266
$wR_2{}^b$	0.0510	0.0579
GOF^c	1.009	1.011

$^a R_1 = \sum ||F_o| - |F_c||/\sum |F_o|$. $^b wR_2 = \{\sum[w(F_o{}^2 - F_c{}^2)^2]/\sum[w(F_o{}^2)^2]\}^{1/2}$. ^{c} GOF $= \{\sum[w(F_o{}^2 - F_c{}^2)^2]/(n - p)\}^{1/2}$, where n is the number of reflections and p is the total number of parameters refined.

true; *g*-tensor true). In the second approach, the ReSpect program package[49] has been employed utilizing the four-component relativistic Dirac–Kohn–Sham (DKS) methodology.[50,51] In this way, the SOC effects are included variationally and thus account for higher than linear effects, which can be especially crucial in calculations of *g*-tensor values of compounds containing heavy elements such as osmium.[52–54] The non-collinear Kramers unrestricted formalism was used as the best method currently available for description of spin polarization at the relativistic DFT level of theory.[51,54,55] The recent implementation of solvent models in the ReSpect program[51] allowed us to take into account the effects of the environment (Me₂SO) in the framework of the COSMO model.

Cell lines and culture conditions

H446 small cell lung carcinoma (American Type Culture Collection, Manassas, VA, USA) and HEK293 embryonic kidney cells (a kind gift from the laboratory of Dr Ross Levine, MSKCC, New York, NY, USA) were maintained in minimal essential medium. 4T1 breast carcinoma (American Type Culture Collection, Manassas, VA, USA) cells were grown in RPMIM. HT-29 colorectal adenocarcinoma cells (a kind gift from the laboratory of Dr Vladimir Ponomarev, MSKCC, New York, NY, USA) were grown in McCoy's medium. All media were supplemented with 10% fetal calf serum, penicillin (100 IU) and streptomycin (100 μg mL^{-1}). All the cell lines were grown in 150 cm^2 culture flasks (Corning Incorporated, New York, NY, USA) under standard sterile cell culture conditions at 37 °C under a humidified atmosphere with 5% CO₂ and 95% air.

Cytotoxicity in cancer cell lines

Cell viability was tested by the Alamar Blue assay (Invitrogen, Carlsbad, CA, USA). Stock solutions of the osmium compounds in Me₂SO were prepared at a concentration of 30 mM. Cisplatin was dissolved in 0.9% aqueous solution of NaCl. Na[*cis*-Os^{III}Cl₄(Hind)₂] (Na[1]) stock solution was prepared under an argon atmosphere to prevent direct contact with oxygen. Serial dilutions of the osmium compounds and cisplatin were prepared in the corresponding nutrient medium, ranging from 0.003 μM to 300 μM. All dilutions contained a final Me₂SO concentration of 1%. For the Alamar Blue assay, cells were plated into 96-well plates (black, clear-bottom, Corning Incorporated) at a density of 4000 cells per well and allowed to adhere for 24 h. Then, the cells were incubated with osmium compounds or vehicle control (medium with Me₂SO) for 48 h. The Alamar Blue reagent was used as described by the manufacturer. The Alamar Blue reagent was diluted 1 : 10 in full culture medium to achieve the working solution. The medium was removed from 96-well plates and 100 μl Alamar Blue reagent was added. The plates were incubated at 37 °C for 3 h under protection from direct light. Fluorescence was read (bottom-read mode) using an excitation wavelength of 570 nm and an emission wavelength of 585 nm on a SpectraMax M5 microplate reader (Molecular Devices, Sunnyvale, CA, USA). The average reading values were analyzed by subtracting the background readings (wells with Alamar Blue but without cells) and compared against the untreated controls of each plate (defined as 100% viability) to determine the percentage of living cells. The experiment was carried out in six parallels of each compound.

Measurement of antiproliferative activity and apoptosis induction

We evaluated the potential of complexes [1] and Na[1] on cell viability, proliferation and apoptosis induction in comparison with *trans*-[Os^{IV}Cl₄(κN1-2*H*-ind)₂] ([3]),[15] cisplatin and untreated cells using an Annexin V Apoptosis Detection Kit (#640914; BioLegend). Thus, we plated 200 000 HT-29 or 4T1 cells per well in 6-well plates. After 24 h medium was removed and the cells were incubated with fresh medium or a 200 μM solution of [1], complex Na[1], [3] or cisplatin in medium for 48 h. After trypsinization, the supernatant and cells were collected in Falcon tubes. 1 ml of the suspension was analyzed in an automated cell counter (Beckman Coulter Counter) for cell count and viability. The remaining cells were stained with a FITC Annexin V (AV) and Propidium Iodide (PI) Kit as described by the manufacturer. The cells were washed twice with cell staining buffer (#420201; BioLegend), resuspended in Annexin binding buffer and transferred to a flow tube with a cell strainer cap (0.2–1 × 10^6 cells in 100 μl). Then, 5 μl Annexin V were added per sample, followed by 10 μl PI. The tubes were incubated for 15 min in the dark and then analyzed on a LSR Fortessa III Flow Cytometer (BD Biosciences). Compensation was carried out using single stained controls. The cells that stained positive for Annexin V were considered early apoptotic, Annexin V and PI positive cells were considered late apoptotic or necrotic and the cells positive only for PI were considered necrotic.

Results and discussion

Synthesis

The complex *cis*-[Os^{IV}Cl₄(κN2-1*H*-ind)₂] ([1]) was prepared by Anderson rearrangement[56] in 1,1,2,2-tetrachloroethane at 128 °C starting from (H₂ind)[Os^{IV}Cl₅(κN1-2*H*-ind)]. This transformation is unprecedented in this family of compounds as it implies both a change of coordination mode from κN1 to κN2 of one indazole ligand and substitution of the chlorido ligand by an outer sphere indazole. The second indazole binds *via* N2 to osmium(ɪᴠ) with the stabilization of the 1*H*-indazole tautomeric form (see Scheme 1).

Starting from (H₂ind)₂[Os^{IV}Cl₆] and by exploring the Anderson-rearrangement reaction, different types of osmium(ɪᴠ) complexes, namely, two coordination isomers, (H₂ind)[Os^{IV}Cl₅(κN1-2*H*-ind)] and (H₂ind)[Os^{IV}Cl₅(κN2-1*H*-ind)], were synthesized. These complexes were studied for their antiproliferative activity *in vitro* and *in vivo* (Scheme 2).[16,57]

Solid state transformation of (H₂ind)₂[Os^{IV}Cl₆] at 150 °C yielded *trans*-[Os^{IV}Cl₄(κN2-1*H*-ind)₂] ([2]) as a side product and *trans*-[Os^{IV}Cl₄(κN1-2*H*-ind)₂] ([3])[15] as the main species (Scheme 3). The minor product 2 could be identified by X-ray diffraction (*vide infra*).
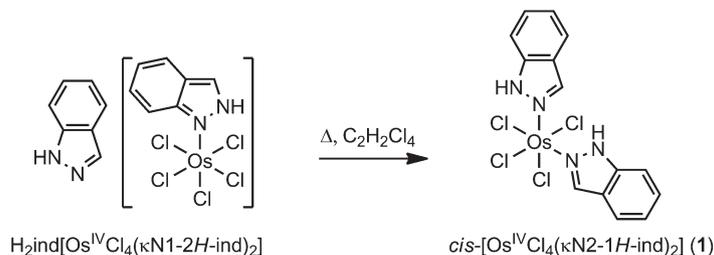
Scheme 1 Synthesis of **1** *via* Anderson rearrangement.
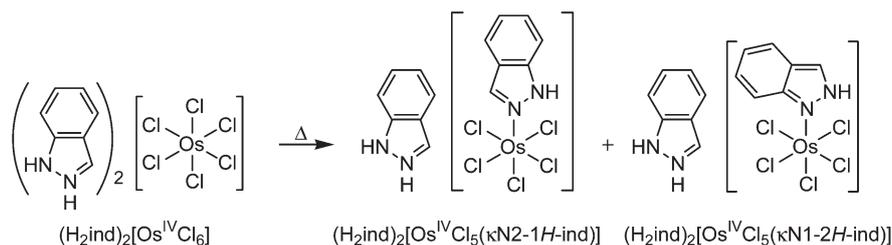
Scheme 2 Synthesis of two linkage isomers of osmium(IV) *via* Anderson rearrangement.
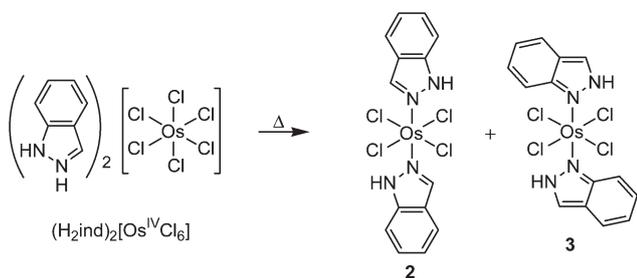
Scheme 3 Synthesis of minor and major products **2** and **3** *via* Anderson rearrangements.

While *trans*-configured osmium analogues of KP1019 in oxidation states +3 and +4, namely [**3**]⁻ and [**3**], have been reported in the literature,[15,29] the corresponding *cis*-compounds were not known. Complex [**3**] was further used for the synthesis of *trans*-[Os^III Cl₄(κN1-2*H*-ind)₂]⁻ ([**3**]⁻) by chemical or electrochemical reduction,[29] building a link between the number of halido ligands, *n*, and Os formal oxidation state: *trans*-[Os^IV Cl₄(Hazole)₂] with $n \geq 4$ and oxidation state +4, and species with $n < 4$ and oxidation state +3, as in *mer*-[Os^III Cl₃(Hazole)₃],[58] *trans*-[Os^III Cl₂(Hazole)₄]Cl, and *cis*-[Os^III Cl₂(Hazole)₄]Cl.[35]

This suggests an associative mechanism for the solid state reaction and a dissociative mechanism for the homogeneous reaction.[59] The reduction of osmium(IV) to osmium(III) with NaBH₄ was performed as described previously for [**3**]⁻ (ref. 29) and [**1**]⁻ was isolated as its tetra-*n*-butylammonium salt (*n*Bu₄N[**1**]). Cation metathesis employing an ion exchange resin[60] afforded the sodium salt Na[**1**]. Compounds [**1**], *n*Bu₄N[**1**], and Na[**1**] were obtained in excellent to good yields of 93, 61, and 62%, respectively.

Crystal structures

The results of X-ray diffraction studies of complexes [**1**]·Me₂CO and [**2**]·2Me₂SO are shown in Fig. 1. Crystallographic data are summarized in Table 1, while selected bond lengths and angles are quoted in Table 2. To the best of our knowledge these are the first tetrachlorido-bis(1*H*-indazole)osmium(IV) complexes to be crystallographically characterized. [**1**]·Me₂CO and [**2**]·2Me₂SO crystallized in the monoclinic centro-symmetric space groups $P2_1/c$ and $P2_1/n$, respectively. The first contains one molecule of *cis*-[Os^IV Cl₄(1*H*-ind)₂] and one molecule of Me₂CO, while the second contains one molecule of *trans*-[Os^IV Cl₄(1*H*-ind)₂] and two molecules of Me₂SO in the asymmetric unit. The osmium atom in [**1**] displays a distorted octahedral coordination geometry with two chlorido ligands and two 1*H*-indazole ligands in equatorial positions, and two chlorido ligands bound axially. In [**2**] osmium(IV) adopts a compressed octahedral coordination geometry with four chlorido ligands occupying the equatorial plane and two 1*H*-indazole ligands in the axial positions. In a few cases reported in the literature, 1*H*-indazole was found to be deprotonated, acting as a bridging ligand in polynuclear metal complexes,[61] or even more rarely it operates as a monodentate indazolato ligand, such as when coordinated *via* N2 to platinum and deprotonated at N1 in the square planar complex [PtCl(*N*-indazolato)(PPh₃)₂].[62]

A comparison of the bond lengths in the coordination sphere of osmium in [**1**], [**2**], and [**3**] is shown in Table 2. Inspection of geometric parameters in complexes [**1**] and [**2**] with the same coordination mode of indazole shows that the Os–N2 and Os–N11 bonds are significantly longer (0.02 Å; $5.5 \times \sigma$) in the *cis*- than in the *trans*-isomer (see Fig. 1 and Table 2). The same trend is clear when the Os–N bonds in *cis*-complex [**1**] are compared to those in *trans*-isomer [**3**] with a
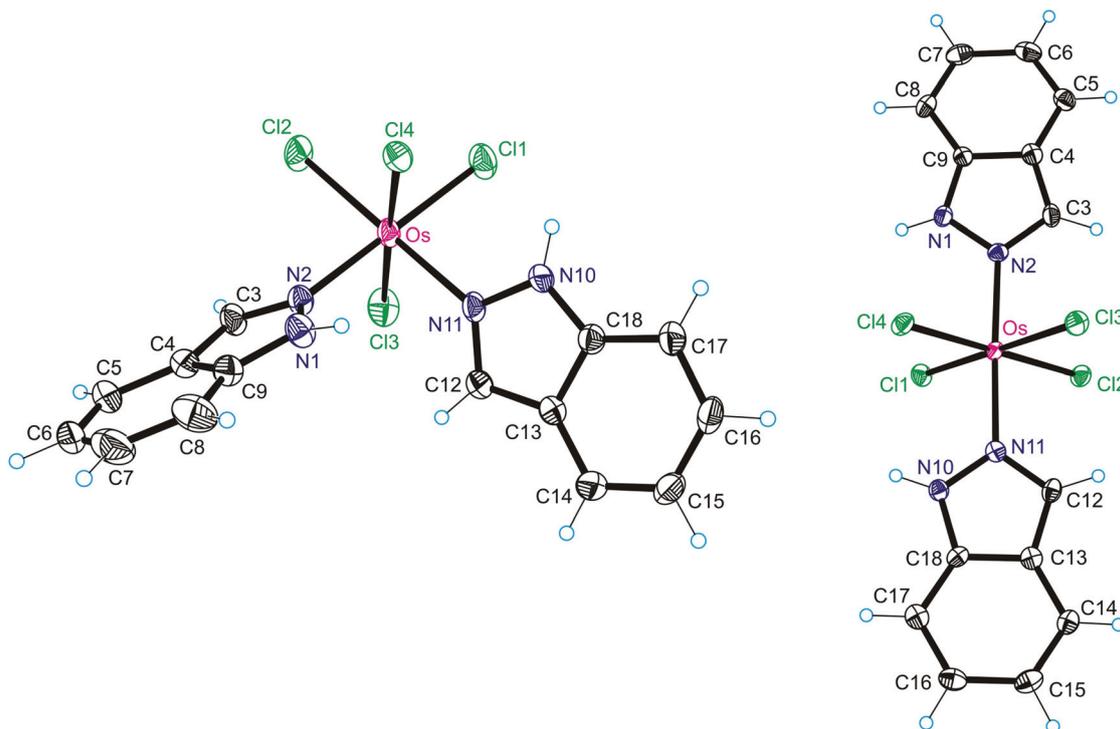
Fig. 1 ORTEP views of [**1**] and [**2**] thermal ellipsoids are drawn at the 50% probability level.

Table 2 Selected bond lengths (Å) and angles (°) in the coordination polyhedron of osmium(IV) in [**1**], [**2**] and [**3**]

Atom1–Atom2	[**1**]·Me₂CO	[**2**]·2Me₂SO	[**3**]
Os–N1			2.050(5)
Os–N2	2.077(2)	2.063(3)	
Os–N11	2.082(2)	2.055(3)	
Os–Cl1	2.3158(6)	2.3022(8)	2.3439(16)
Os–Cl2	2.3174(6)	2.3222(9)	2.3395(15)
Os–Cl3	2.2974(7)	2.3099(8)	
Os–Cl4	2.3251(6)	2.3197(9)	
N1–N2	1.358(3)	1.357(4)	
Atom1–Atom2–Atom3			
N1–Os–Cl1			91.73(15)
N1–Os–Cl2			89.32(15)
N2–Os–N11	90.51(8)	177.52(10)	
N2–Os–Cl2	89.54(6)	89.99(8)	
Cl1–Os–Cl2	90.85(2)	89.82(3)	90.22(6)
Cl1–Os–N11	89.09(6)	91.78(8)	
Cl1–Os–Cl4	90.30(2)	90.36(3)	
N11–Os–Cl4	87.42(6)	90.87(8)	
N2–Os–Cl4	89.01(6)	90.23(8)	
Cl2–Os–Cl4	91.91(2)	179.72(3)	

dissimilar coordination mode of indazole (see Chart 2). This is presumably due to a stronger *trans*-influence of the chlorido ligand compared to nitrogen atom N2 or N1 (using the numbering for indazole in Chart 1) of indazole. Interestingly, an insignificant (<3 × σ) shortening of axial Os–N bonds in *trans*-complex [**3**] compared to that in *trans*-complex [**2**] (coordination modes are different) results in a significant (14 × σ) lengthening of equatorial Os–Cl bonds by *ca.* 0.03 Å (see Table 2) in [**3**] *vs.* those in [**2**].

Both *trans*-indazole ligands in [**2**] are almost coplanar in contrast to what was found in (Ph₄P)[*trans*-RuCl₄(1*H*-indazole)₂], wherein the 1*H*-indazole ligands were significantly twisted.[63] The plane through both azole ligands crosses the equatorial plane between chlorido ligands, the torsion angles $\Theta_{Cl1-Os-N1-N2}$ and $\Theta_{Cl2-Os-N2-N1}$ being −30.4(4) and −47.8(2)°, respectively.

A salient structural feature is the stabilization of indazole in its usual 1*H*-indazole form in [**1**] and [**2**] (Fig. 1) and coordination to osmium *via* nitrogen atom N2. This mode of coordination is typical of other metal ions, *e.g.* ruthenium, but rare for osmium(IV). The only previous example for osmium, namely H₂ind[Os^{IV}Cl₅(1*H*-ind)], was reported by some of us recently.[57]

Intermolecular hydrogen bonding interaction between complexes [**1**] and [**2**] and co-crystallized solvent molecules are shown in Fig. S2 and S3 in the ESI.‡

NMR spectra

All compounds were characterized by ¹H NMR spectra showing signals due to the coordinated indazole. In the spectrum of *n*Bu₄N[**1**], signals of the Bu₄N⁺ cation could also be assigned. The paramagnetic osmium(IV) in [**1**] caused some line broadening and spread of chemical shifts from −9.42 to +16.49 ppm (Fig. S4‡). It should, however, be noted that despite the paramagnetism of osmium(IV) in [**1**], the NMR lines remain sharp enough such that coupling constants could be easily determined. Qualitatively, the fact that the nuclear paramagnetic resonance spectrum of [**1**] is readily interpretable is unsurpris-

ing for Os^{IV} (low-spin (LS) $5d^4$, $S = 1$) because this ion is expected to have very fast electron spin relaxation[64] due to the substantial orbital angular momentum of its ground state and the extremely large spin–orbit coupling (SOC) constant of Os^{IV} (free-ion $Os^{4+}_{(g)}$ (Os(v) in spectroscopic notation) has $\zeta_d = 4133.7$ cm^{-1});[65] ions with slow electronic relaxation, such as high-spin (HS) $3d^5$ $S = 5/2$ (*e.g.*, Fe^{III}), in contrast, typically give unusable NMR spectra.[64] The number of carbon resonances in ^{13}C NMR spectra of [1] is in agreement with C_2 molecular symmetry of the complex. The broadening of resonances due to paramagnetism of osmium(III) (low-spin $5d^5$ $S = 1/2$) in nBu_4N [1] and Na[1] is more obvious compared to that for [1] and signal splitting for indazole protons is no more discernible. All signals are significantly upfield shifted being in the δ range from 3.55 to -22.16 ppm.

UV–vis spectra and solvatochromism

The UV–vis spectra of [1] have been measured in a number of organic solvents (Fig. 2). Depending on the solvent used, a red shift of the absorption maximum from 543 (THF) to 618 (Me$_2$SO) nm was observed. This is in line with the relative permittivity values (ε_r) of solvents used [tetrahydrofuran (7.5),[66] acetone (21.30),[67] ethanol (25.02),[67] acetonitrile (38),[68] dimethyl formamide (37.31),[69] dimethyl sulfoxide (47.2)].[70] This can be explained by the better stabilization of (polar) excited states by likewise polar solvents.

Electrochemical behavior

The cyclic voltammogram of [1] in a solution of 0.2 M nBu_4NPF_6 in acetonitrile starting from the anodic part using a platinum wire as the working electrode and a scan rate of 0.2 V s^{-1} is shown in Fig. 3.

The first reduction step is reversible ($E_{1/2} = 0.69$ V *vs.* NHE or $+0.01$ V *vs.* Fc$^+$/Fc) at all scan rates used (from 10 mV s^{-1} to 500 mV s^{-1}), and is followed by the less reversible one at a more negative potential ($E_{1/2} = -0.78$ V *vs.* NHE). Upon *in situ* reduction at a scan rate of 10 mV s^{-1} in the region of the first reversible cathodic peak in acetonitrile, the UV-vis absorption
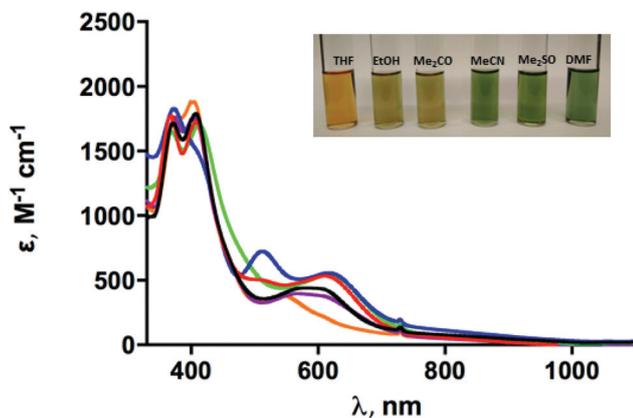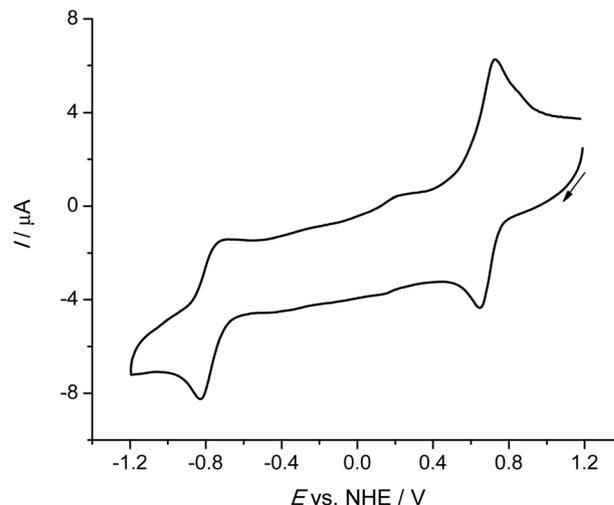

Fig. 3 Cyclic voltammogram of *cis*-[Os^{IV}Cl$_4$(κN2-1H-ind)$_2$] ([1]) in 0.2 M nBu$_4$NPF$_6$ in acetonitrile at a platinum working electrode (scan rate 0.2 V s^{-1}).

bands at 408, 370 and 272 nm decreased, and, simultaneously, a new dominating band at 318 nm appeared (Fig. 4a). Fully reversible spectroelectrochemical behavior confirmed the high stability of cathodically generated *cis*-[Os^{III}Cl$_4$(κN2-1H-ind)$_2$]$^-$ ([1]$^-$) species. A very similar reversible cyclic voltammetric and spectroelectrochemical response was observed for [1] also in Me$_2$SO at the first reduction peak even at a very low scan rate of 5 mV s^{-1} as illustrated in Fig. S5.‡ Here the UV-vis absorption bands of [1] in Me$_2$SO at 415, 370 and 280 nm decreased, and, simultaneously, a new dominating band at 325 nm was observed. The spectroelectrochemical data indicated that the isolation of the osmium(III) species in the solid state after reduction of the parent osmium(IV) complex is feasible. The chemically prepared and isolated osmium(III) complex nBu_4N [1] can be easily oxidized in Me$_2$SO back to [1]^0 at anodic potential $E = +1.0$ V *vs.* NHE as shown in Fig. S6.‡

Fig. 4c shows the absorption spectra of the initial *cis*-isomer [1] (cyan trace) and one-electron reduced species, namely ([1]$^-$) (dark yellow trace). The UV–vis spectrum of the osmium(III) species [1]$^-$ generated electrochemically exhibits an absorption maximum at a slightly higher wavelength (318 nm in acetonitrile and 325 nm in Me$_2$SO) compared to its analogue *trans*-[Os^{III}Cl$_4$(κN1-2H-ind)$_2$]$^-$ ([3] in Me$_2$SO) reported previously[29] with λ_{max} at 301 nm. Of note is a more negative reduction potential with a shift of -200 mV reported recently for [3][29] with $E_{1/2} = +0.49$ V *vs.* NHE or $E_{1/2} = -0.19$ V *vs.* Fc$^+$/Fc for the first reduction step. A significant difference in the $E_{1/2}$ values for [1] and [3] indicates a stronger effect of *cis/trans* isomerism on reduction potentials than that of the coordination mode of indazole in the compared species.

As mentioned previously, the Os$^{III/II}$ couple is much less reversible than the Os$^{IV/III}$ couple and takes place at much more negative potentials. Upon repetitive redox cycling of sample 1 going up to the voltage of the second reduction peak,

Fig. 2 UV-vis spectra of solutions of [1] in Me$_2$CO (black), acetonitrile (red), DMF (blue), Me$_2$SO (green), ethanol (purple) and THF (orange).
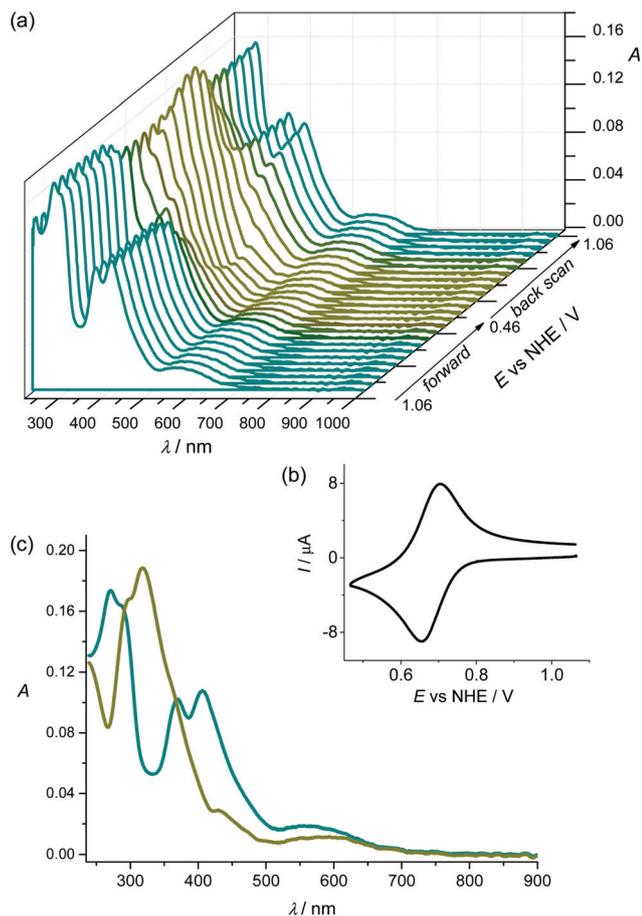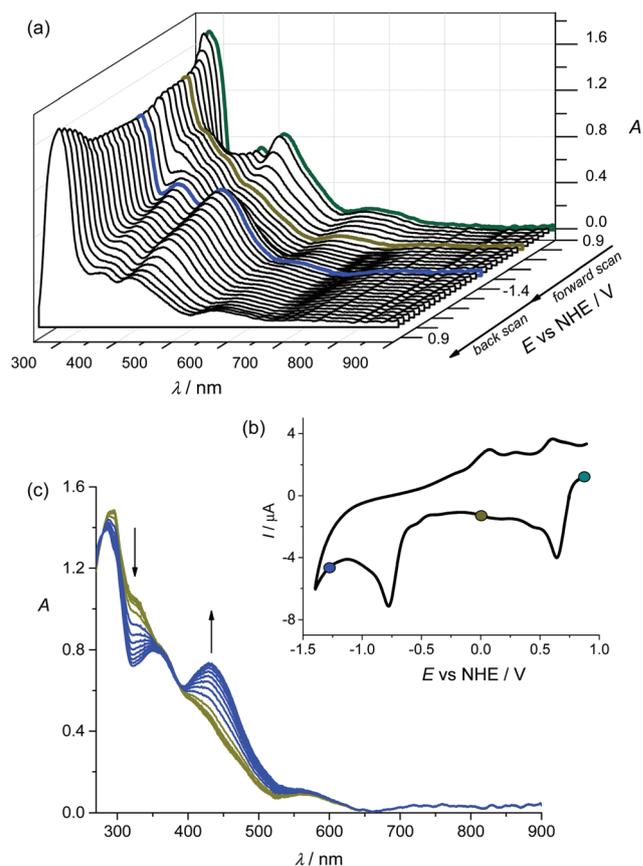
Fig. 4 UV-vis spectroelectrochemistry of [**1**]. (a) Electrochemical potential dependence of optical spectra. (b) The corresponding cyclic voltammogram (0.2 M nBu$_4$NPF$_6$ in acetonitrile, scan rate 10 mV s^{-1}). (c) Optical spectrum of [**1**] in 0.1 M nBu$_4$NPF$_6$/acetonitrile before (dark cyan trace) and after cathodic reduction at the first reduction peak (dark yellow trace – UV-vis spectrum measured at 0.46 V *vs.* NHE).

Fig. 5 *In situ* UV-vis spectroelectrochemistry of [**1**] in 0.2 M nBuN$_4$[PF$_6$] in Me$_2$SO (scan rate 5 mV s^{-1}): (a) UV-vis spectra observed upon cyclic voltammetry of [**1**] going to the second reduction peak. (b) The corresponding *in situ* cyclic voltammogram (selected colored UV-vis spectra in (a) correspond to the potentials marked with the colored circles in the voltammogram); (c) UV-vis spectra detected simultaneously upon the reduction of [**1**] in the region of the second cathodic peak (from −0.5 to −1.3 V *vs.* NHE).

irreversible changes were observed in cyclic voltammetric experiments in the thin layer cell at a scan rate of 10 mV s^{-1} both for Me$_2$SO and acetonitrile solutions as illustrated in Fig. S7.‡ New redox active species are formed during the reduction of [**1**]$^-$ in the region of the second electron transfer indicating a lower stability of the generated osmium(II) complex. The changes in UV-vis spectra observed during cyclic voltammetry of [**1**]$^-$ going to the region of the second reduction in the Me$_2$SO solution (scan rate 5 mV s^{-1}) are shown in Fig. 5. A new optical band arises at *ca.* 440 nm in the region of the second electron transfer (see Fig. 5c and Fig. S8 and S9‡) which again disappears upon reoxidation. The irreversible changes in the initial optical spectra of [**1**] were observed confirming the irreversible chemical changes of the corresponding osmium(II) species [**1**]$^{2-}$ formed upon cathodic reduction of [**1**] at the second reduction step. Interestingly, a newly formed product can be reversibly reduced at $E_{1/2} = +0.27$ V *vs.* NHE (see blue trace in Fig. S7‡). Cathodically induced metal dechlorination was previously mentioned for the *trans*-

[Ru^{III}Cl$_4$(Hind)$_2$]$^-$ complex[71] upon reduction of ruthenium(III) to ruthenium(II) and for the *trans*-Os^{III} analogues.[29] Similarly, our findings indicate that a chlorido ligand is replaced by a solvent molecule upon reduction of osmium(III) species and a new redox active osmium(II) complex containing a coordinated solvent molecule is formed at the second reduction potential of [**1**]^0 (respectively at the first reduction peak for [**1**]$^-$).

EPR of osmium(III) complexes

As mentioned previously, the NMR resonances of the osmium(III) complexes nBu$_4$N[**1**] and Na[**1**] were considerably broadened due to the rapid nuclear relaxation induced by the paramagnetism of these compounds, which could be expected from the LS d^5 electron configuration of the central metal.[33b,c] EPR is a valuable technique to unravel the underlying mechanisms of action of paramagnetic anticancer drugs and, in particular, those of ruthenium(III).[31] The X-band EPR spectra of frozen solutions of nBu$_4$N[**1**] (in Me$_2$SO at 94 K) and Na[**1**] (in H$_2$O/ethylene glycol 5 : 1 v/v at 12 K) are shown in Fig. 6 and
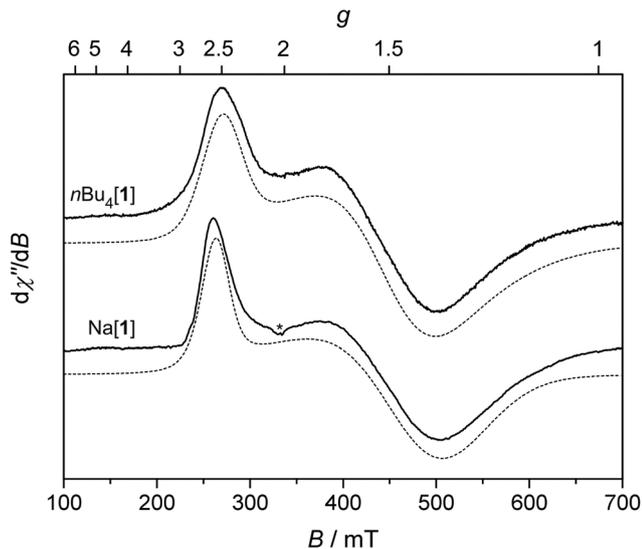
Fig. 6 (Top) X-band (9.436 GHz) EPR spectrum of nBu$_4$N[**1**] in Me$_2$SO recorded at 94 K (solid trace) together with the simulation (dashed trace). (Bottom) X-band (9.362 GHz) EPR spectrum of Na[**1**] in H$_2$O/ethylene glycol 5 : 1 v/v recorded at 12 K (solid line) together with the simulation (dashed line). Spin Hamiltonian parameters are listed in Table 3. * denotes the signal from an impurity.

confirm the paramagnetic nature of the complexes, while a Q-Band EPR spectrum of Na[**1**] and a powder EPR spectrum of nBu$_4$N[**1**] are shown in Fig. S10 and S11,‡ respectively.

Both spectra show rather broad lines with $\Delta B_{pp} > 150$ mT and not a very well resolved spectral pattern, characterized by a rhombic g-tensor.[72] The g values obtained by the simulation of the spectra (Table 3, $g_{max} \approx 2.50$, $g_{mid} \approx 1.45$ and $g_{min} \approx 1.35$) are very similar and can be considered virtually identical for both complexes, if we take into account the uncertainty of g-value determination induced by the large linewidth. Thus the cis-[Os^{III}Cl$_4$(κN2-1H-ind)$_2$]$^-$ complex anion geometry in frozen solution as well as the electronic configuration are not influenced by the different counterions that govern the solubility of nBu$_4$N[**1**] and Na[**1**] in an organic or aqueous environment, respectively. An unambiguous conclusion about the spin state of a complex cannot be made based solely on a single frequency cw-EPR experiment.[73] However, the interactions between the unpaired electrons in the high spin states

Table 3 The g-values of Os^{III} complexes nBu$_4$N[**1**], Na[**1**] obtained from simulation of their EPR spectra

g-Factor[a]	nBu$_4$N[**1**][b]	Na[**1**][c]
g_{max}	2.44 ± 0.05	2.50 ± 0.05
g_{mid}	1.44 ± 0.05	1.45 ± 0.05
g_{min}	1.31 ± 0.05	1.37 ± 0.05

[a] While EPR is unable to provide the absolute sign of the g factor the ligand field theory analysis indicates that the g values are all negative for the investigated complexes (see Table 4). The assignment of g-tensor component directions is not made here; only ordering by magnitude (see Table 4 for such assignments). [b] In Me$_2$SO at 94 K. [c] In H$_2$O/ethylene glycol 5 : 1 v/v at 12 K.

usually result in a facilitated electron spin relaxation, and the consequent line broadening renders their EPR spectra often undetectable above liquid helium temperatures. The fact that we were able to record the spectrum of nBu$_4$N[**1**] at 94 K and a comparable linewidth was observed in the spectrum of Na[**1**] at 12 K, indicate the absence of such electron–electron interactions. Moreover, the 35 GHz EPR spectrum of Na[**1**] (Fig. S10‡) confirms the g_{max} value from X-band. The osmium(III) ion is thus in the usual low spin d^5 ($S = \frac{1}{2}$) configuration, in both nBu$_4$N[**1**] and Na[**1**], as reported for the vast majority of Os^{III} complexes in the literature.[33a,b]

Ligand field theory discussion of ^{2}[**1**]$^-$ g-tensor

The g values of LS nd^5 complexes have been extensively analyzed over the years because of the importance of this electronic configuration in heme proteins and other bioinorganic systems.[74] The model that we shall use for a simple ligand-field theory (LFT) analysis of the g tensor of ^{2}[**1**]$^-$ is that developed by McGarvey.[33b,c] The details need not be discussed here, but the model treats this t$_{2g}^5$e$_g^0$ configuration (strong-field notation) by ignoring any effects of excited states involving the e$_g$ orbitals and using the "hole" in the t$_{2g}$ orbitals as a basis set as follows:[75]

$$|xy, \pm 1/2\rangle = d_{xz}^+ d_{xz}^- d_{yz}^+ d_{yz}^- d_{xy}^\pm;$$
$$|xz, \pm 1/2\rangle = id_{yz}^+ d_{yz}^- d_{xy}^- d_{xy}^- d_{xz}^\pm;$$
$$|yz, \pm 1/2\rangle = d_{xz}^+ d_{xz}^- d_{xy}^+ d_{xy}^- d_{yz}^\pm.$$

The (axial) splitting between the d$_{xy}$ and d$_{xz,yz}$ orbitals is given by Δ and the (rhombic) splitting between the d$_{xz}$ and d$_{yz}$ orbitals is given by V. This analysis has been used previously for Ru^{III} complexes of general type $trans$-[Ru^{III}(NH$_3$)$_4$(L)(L')]$^{n+}$,[76] which could be considered as cationic analogues to the equatorially tetrachlorido coordinated anionic Ru/Os^{III} complexes. To the best of our knowledge, no EPR spectra of complexes of general formula cis-[Os^{III}X$_4$(L)(L')] have been reported. Clarke and co-workers have reported EPR spectra for cis-[Ru^{III}(NH$_3$)$_4$(Him)$_2$]Br$_3$.[77] It is possible to use analytical equations given by McGarvey to extract an internally consistent set of LFT parameters from the experimental g values.[78] This has been done here and the results are given in Table 4. In each case, there are two solutions, but usually, one can be discarded as it requires unreasonable parameters, $e.g.$, the orbital reduction factor, k, is much too far from 1.0, or the splitting among the t$_{2g}$ orbitals is much too large. Note that in this model it is not possible to provide the absolute energy splitting among the t$_{2g}$ orbitals, only their energies normalized by the spin–orbit coupling (SOC) constant, ζ. This parameter has recently been accurately determined for free-ion Os^{3+}$_{(g)}$ (Os IV in spectroscopic notation) in its 5d^5 electronic configuration: $\zeta_d = 3738.6$ cm^{-1}.[79] The reduction of this parameter due to covalency in these complexes is unknown, but values of $\zeta = 2530$ and 2220 cm^{-1} in $trans$-[OsCl$_4$(CO)(py)]$^-$ (py = pyridine) are found respectively for Cs$^+$ and tetraethylammonium countercations.[34] The fact that the SOC constant is so sensitive even to counterions indicates the difficulty of quantifying this interaction, but an estimate of $\zeta \approx 2500$ cm^{-1} seems reasonable in

Table 4 The g-values of Ru[III] and Os[III] complexes relevant to the present work with results from LFT analysis

Complex[a]	g_x, g_y, g_z [i]	Δ/ζ [h]	V/ζ [h]	V/Δ	k
nBu4N[1]	−1.31, −1.44, −2.44	−0.492	−0.043	0.088	0.8204
Na[1]	−1.37, −1.45, −2.50	−0.498	−0.026	0.053	0.8541
trans-[OsCl$_4$(CO)(py)]$^-$ ^{b}	−2.55, −2.55, −1.72	+0.228	0.0	0	1.220
trans-[OsBr$_4$(CO)(py)]$^-$ ^{b}	−2.50, −2.50, −1.80	+0.236	0.0	0	1.211
trans-[OsBr$_4$(CO)$_2$]$^-$ ^{b}	−2.46, −2.46, −1.81	+0.221	0.0	0	1.192
trans-[RuCl$_4$(Him)$_2$]$^-$ ^{c}	−3.12, −2.44, −1.2	+0.536	+0.316	0.589	1.256
trans-[RuCl$_4$(Me$_2$SO)$_2$]$^-$ ^{d}	−2.35, −2.35, −1.87	+0.166	0.0	0	1.148
trans-[Ru(NH$_3$)$_4$(Him)$_2$]$^{3+}$ ^{e}	−3.04, −2.20, (−0.15); −3.04, −2.20, (+0.15); (−0.9), −2.20, −3.04; (+0.9), −2.20, −3.04	+0.9635; +1.136; −0.6392; −1.847	+0.6043; +0.7123; −0.4016; −1.160	0.627; 0.627; 0.628; 0.628	1.002; 0.9667; 1.114; 0.9270
cis-[Ru(NH$_3$)$_4$(Him)$_2$]$^{3+}$ ^{e}	−2.88, −2.14, (−0.65); −2.88, −2.14, (+0.65); −2.88, −2.14, (−0.15); −2.88, −2.14, (+0.15)	+0.6905; +1.463; +0.9253; +1.094	+0.4265; +0.9017; +0.5357; +0.6328	0.618; 0.616; 0.579; 0.579	1.003; 0.8360; 0.9255; 0.8858
[Os(NH$_3$)$_5$(H$_2$O)]$^{3+}$ ^{f}	−2.3, −2.3, −1.22; −2.2, −2.2, −1.08	+0.3855; +0.4097	0.0; 0.0	0.0; 0.0	0.9795; 0.8954
[Ru(NH$_3$)$_5$(H$_2$O)]$^{3+}$ ^{g}	−2.620, −2.620, −0.6; −2.620, −2.620, (0.0)	+0.7119; +0.9878	0.0; 0.0	0.0; 0.0	1.052; 0.9678
trans-[Ru(NH$_3$)$_4$(4-pic)(H$_2$O)]$^{3+}$ ^{h}	−1.20, −1.56, −2.81	−0.671	−0.112	0.167	0.9378

^{a} Counterions are not given except for the two Os[III] complexes reported here, but are noted for others below when relevant. ^{b} Taken from Kremer;[34] py = pyridine. The g values presented are all for complexes with tetraethylammonium countercation; for trans-Cs[OsCl$_4$(CO)(py)]: $g_\perp$ = 2.46, $g_\parallel$ = 1.45. ^{c} Taken from Ni Dhubhghaill et al.[82] ^{d} Taken from de Paula et al.[80] The g values reported are for the solid material; in aqueous or methanol solution, multiple species are reported due to replacement of Me$_2$SO and/or chlorido ligands by solvent. ^{e} Taken from Clarke et al.[77] The values for $|g_{min}|$ were not observed (hence they are given in parentheses), but were proposed by their LFT analysis. In these systems, the proper choice of sign of the g values is not apparent based on standard criteria, namely the magnitudes of k or Δ, so both choices are given. The results of additional calculations are given; for the trans complex, using a value for $|g_{min}|$ that would likely be the largest possible, but difficult to observe experimentally: $|g_{min}|$ = 0.9; for the cis complex using the a value for $|g_{min}|$ that would likely be the smallest possible: $|g_{min}|$ = 0.15 (a value of zero is possible, but does not provide enough information for the fitting process). We favor the first entry listed in each case, which is in agreement with the model originally favored by Clarke et al. ^{f} Taken from McGarvey et al.[33c] Two species are always observed in frozen aqueous solutions of [Os(NH$_3$)$_5$(H$_2$O)](CF$_3$SO$_3$)$_3$. ^{g} Taken from McGarvey et al.[33c] The experimentally reported range for $|g_{min}|$ is 0.0 ≤ $|g_{min}|$ ≤ 0.6; we thus present calculations for both 0.6 and 0.0 – the minimum magnitude. ^{h} Taken from Souza et al.;[32] 4-pic = 4-picoline (4-methylpyridine). The specific g values reported are those for frozen aqueous/ethylene glycol solution; those for a powder and in other solvents were similar. ^{i} The signs of the g values are not determined experimentally, but are determined here by the model of McGarvey,[33b] which provides two choices of sign. Only the more physically plausible choice of signs is presented, except when both choices are acceptable.

our case (reduction by roughly one third of the free-ion value), so it can be used to convert the calculated Δ/ζ and V/ζ values into estimates of ligand-field splittings. It should also be noted that all of the trans-[OsX$_4$(L)(L′)]$^-$ (X = Cl, Br and I; L = CO; L′ = CO and py) complexes studied by Kremer gave axial EPR spectra. This is a consequence of the linear (cylindrical π-bonding) binding of the CO ligand to osmium. Axial EPR spectra are also seen for complexes of type trans-[RuCl$_4$(L)(Me$_2$SO)]$^-$, where L = Me$_2$SO[80] or various azole ligands, e.g., pyrazole, as well as pyridine.[81] The key point, however, is not that whether a (Ru,Os)[III] species exhibits a rhombic or axial spectrum, but whether $g_\parallel$ (i.e., the unique feature) is greater (at lower resonant magnetic field) or lesser (at higher field) than $g_\perp$ (averaging a rhombic signal if necessary). In general, the (Ru,Os)[III] species listed in Table 4 exhibit $|g_\parallel| < |g_\perp|$, but [1]$^-$ shows the reversed g value ordering.

McGarvey has explained the electronic structure of trans-[MX$_4$(Y$_2$,YZ)] complexes (where M = Ru[III] most commonly) in terms of an angular overlap model (AOM) wherein the z axis is along Y–M–Y(Z) and the relevant AOM parameter is π-bonding between the metal ion and each ligand type, $\varepsilon_\pi(X, Y, Z)$, so that $\Delta = 2\varepsilon_\pi(X) - [\{2\varepsilon_\pi(Y)\}, \{\varepsilon_\pi(Y) + \varepsilon_\pi(Z)\}]$. McGarvey showed that this model works reasonably well for simple complexes such as trans-[RuCl$_2$(NH$_3$)$_4$]$^+$. More relevant here, the model also works

qualitatively for trans-[OsBr$_4$(CO)$_2$]$^-$: the bromido ligands are expected to be π-donors (i.e., $\varepsilon_\pi(X) > 0$) and the carbonyl ligands are expected to be strong π-acceptors (i.e., $\varepsilon_\pi(Y) < 0$). This would give $\Delta > 0$, consistent with what is obtained from the g value analysis. No cis-[MX$_4$(Y$_2$,YZ)] complexes were known to McGarvey, but he proposed that $\Delta = -\varepsilon_\pi(X) + \varepsilon_\pi(Y)$ for this geometry.[33b] The chlorido ligands (X) are expected to be π-donors and the indazole nitrogen atoms (Y) are expected to be weak π-acceptors $\varepsilon_\pi(Y) \lesssim 0$, which would give $\Delta < 0$, again consistent with the g values.

A further discussion of the LFT parameters of these complexes is beyond the scope of this study, and would be in any case risky due to the overall relatively small number of Os[III] coordination complexes characterized by EPR, and in particular, the lack of data on other Os[III] cis/trans isomers. However, it is clear that the cis-Os[III] complex, [1]$^-$, as manifest in its "reversed" EPR spectrum, exhibits an electronic structure distinctly different from almost all of the related species listed in Table 4, in particular the trans-Os[III] complexes. The wavefunction coefficients resulting from this analysis show that the "hole" is primarily in the d$_{xz}$ and d$_{yz}$ orbitals in the present system, while it is primarily in the d$_{xy}$ orbital in most other cases. The exception is [Ru(NH$_3$)$_4$(4-pic)(H$_2$O)]$^{3+}$ (4-pic = 4-picoline (4-methylpyridine)) wherein competing π-bonding involving the trans ligands was proposed to lead to the change in the

Table 5 Results of the theoretical determination by quantum chemical theory calculations of the g-tensor compared with experimental data

| Method	g_x	g_y	g_z	Details
EXP. (94 K)	1.31	1.44	2.44	Me$_2$SO
EXP. (12 K)	1.37	1.45	2.50	H$_2$O/ethylene glycol 5 : 1 v/v
ZORA/BLYP	2.056	3.649	5.087	*In vacuo*
	2.030	4.731	5.507	COSMO(Me$_2$SO)
ZORA/B3LYP	2.041	4.428	5.094	*In vacuo*
	2.021	4.908	7.258	COSMO(Me$_2$SO)
ZORA/CASSCF	1.665	1.780	3.090	*In vacuo*
	1.594	1.702	3.188	COSMO(Me$_2$SO)
DKS/B3LYP	0.729	2.002	2.536	*In vacuo*
	1.262	1.797	2.471	COSMO(Me$_2$SO)

electronic ground state.[32] A quantum chemical theory (QCT) treatment presented in the next section provides further insight into [**1**]⁻.

Theoretical determination of ²[**1**]⁻ g-tensor

QCT calculations of EPR parameters of compounds containing heavy elements are challenging due to a dominating importance of spin–orbit relativistic effects. While in the case of compounds containing 3d transition metal complexes it is

sufficient to treat the relativistic SOC effects in the evaluation of the g-tensor as a perturbation of the non-relativistic wave-function,[44] in the case of 4d- and 5d-transition metal compounds the explicit inclusion of both scalar and SOC relativistic effects[83] appears necessary.[51–55] Herein, we wish to compare the performance of the g-tensor evaluation of ²[**1**]⁻ using a perturbative inclusion of SOC in the scalar relativistic ZORA wavefunction using either DFT or CASSCF levels of theory[44] with the rigorous treatment of relativistic effects and g-tensor evaluation at the DKS level.[51–55] Furthermore, the solvent polarization effects will be considered for further consistency *via* the COSMO approach.

The calculated g-tensor values are shifted from the experimental ones in the case of scalar ZORA DFT calculations with the perturbative inclusion of SOC. The solvent effects are large within the ZORA DFT treatment but do not lead to improvement with respect to experiments (Table 5). Considerably better agreement is achieved in the case of ZORA CASSCF calculations which yield a semi quantitative agreement with experiment [both *in vacuo* and *via* the COSMO(Me$_2$SO) solvent model]. Nevertheless, the CASSCF setup has been kept under conservative settings for the rotations out of the active space to enforce the d-electronic configuration of the open shell and/or
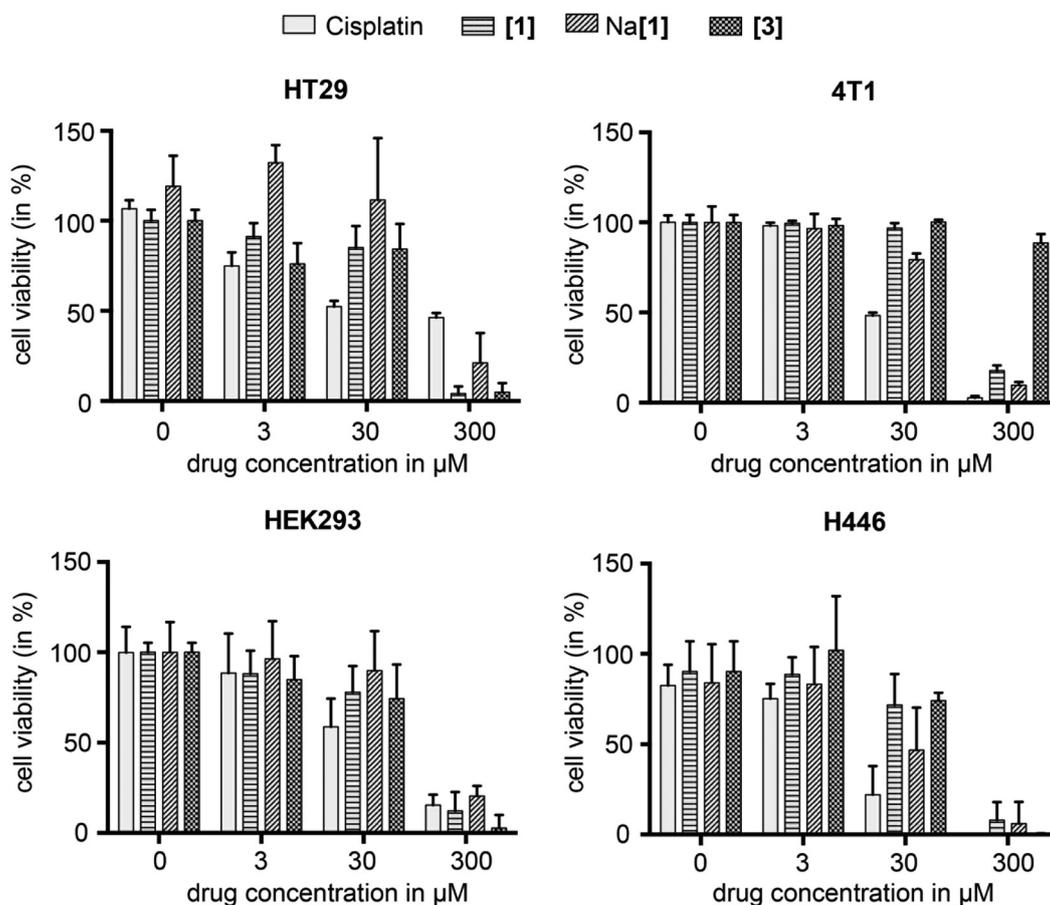
Fig. 7 Cell viability of human cancer cell lines after a 48 h treatment with cisplatin, [**1**], Na[**1**] and [**3**], in relation to the untreated control (1% Me$_2$SO) using the Alamar Blue assay kit. Displayed are means ± standard deviation of six parallels.

in the active space. Although the rigorous DKS method does not yield the best agreement *in vacuo*, introducing a solvent model leads to a large improvement of the calculated results providing almost quantitative agreement with the experiment. This once again shows the need for a suitable treatment of both relativistic and spin polarization effects in the calculation of EPR parameters for 5d ions. As such, the calculated solvent effects on the electronic *g*-tensor parameters are so far the largest ones observed at the DKS level of theory and to the best of our knowledge, they are the largest ones calculated for systems containing heavy elements. Furthermore, the excellent agreement of DKS/COSMO theory with experimentally determined values is promising for a more systematic theoretical exploration of experimentally determined *g*-tensors for osmium(III) compounds,[34] and potentially other paramagnetic 5d[5] ion complexes, such as of rhenium(II)[84] or iridium(IV).[85]

Effective concentrations to affect cell viability

Having now the availability of well-characterized *cis*- as well as *trans*-osmium(III) complexes it is possible to make a direct comparison of their anti-cancer efficacy. Specifically, first to determine in which concentration range these complexes mediate cytotoxic effects, we conducted a cytotoxicity screen in four different cancer cell lines (HT29, 4T1, HEK293 and H446) and compared the effects to an untreated control and cispla-

tin. The results for select drug concentrations are displayed in Fig. 7. Strong effects on cell viability were only observed for the highest concentration of 300 μM, where all cell lines showed a viability of below 30% compared to the control, with the exception of 4T1 cells to treatment with *trans*-[Os^{IV}Cl$_4$(kN1-2*H*-ind)$_2$] ([3]). At 30 μM cisplatin reduced cell viability to 30–60%, while the osmium compounds did not reduce viability. HT29 cells were the only cells where the osmium compounds led to a stronger reduction of cell viability than cisplatin. The corresponding IC$_{50}$ values are quoted in Table S1.‡

Antiproliferative activity in cancer cell lines

We further determined the potential of complexes [1] and Na[1] to inhibit proliferation and induce apoptosis in comparison with *trans*-[Os^{IV}Cl$_4$(κN1-2*H*-ind)$_2$] ([3]) and cisplatin in HT29 and 4T1 cells at a concentration of 200 μM. Here, we used an apoptosis detection kit to quantify the percentage of a cell population that has entered an early apoptotic (AV+/PI−) or late apoptotic/necrotic state (AV+/PI+) using flow cytometry (Fig. 8a). We found that the 4T1 (breast cancer) cells were very sensitive to cisplatin (more than 60% increase in AV+ and AV+/PI+ cells compared to untreated cells), while HT29 (colorectal) cells showed no significant difference between untreated and cisplatin treated cells (Fig. 8b). Interestingly, the cisplatin resistant HT29 cells were more sensitive to treatment
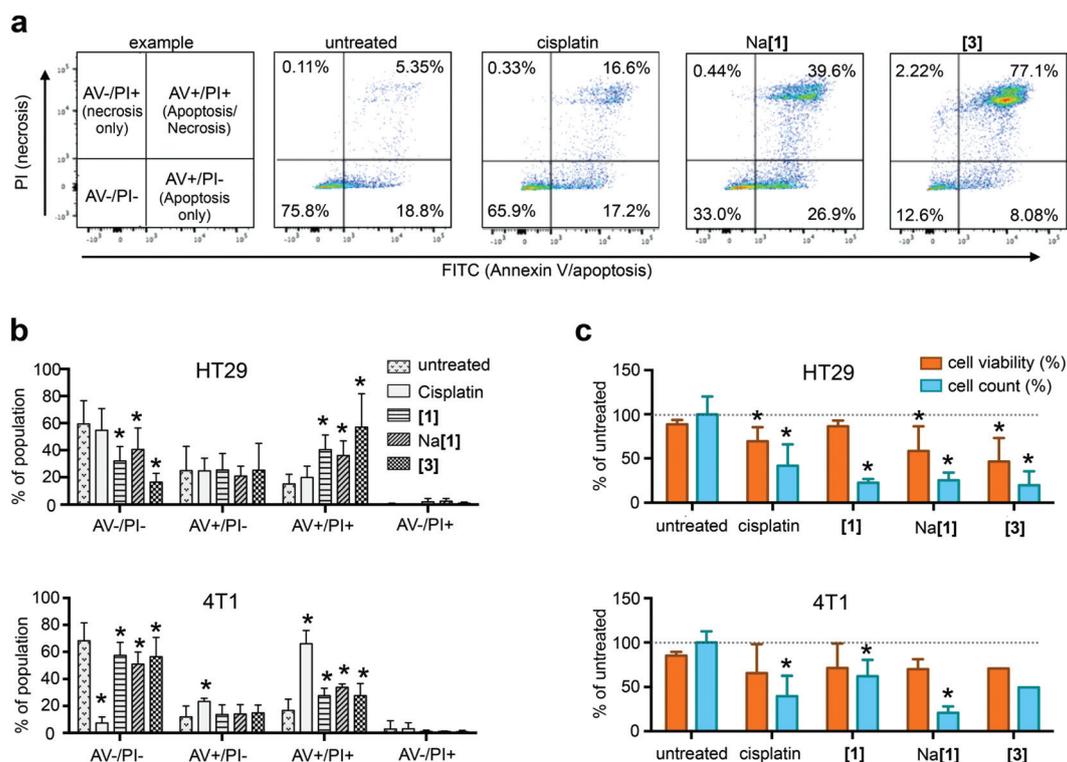
Fig. 8 Antiproliferative effects of treatment with 200 μM cisplatin, [1], Na[1] or [3], on HT29 and 4T1 cancer cell lines. (a) Example of discriminability of apoptotic and necrotic cell populations in HT29 cells after a 48 h treatment using a flow cytometry assay. (b) Quantification of early apoptotic and late apoptotic/necrotic cell populations in treated and untreated cells. (c) Relative cell viability and cell number after a 48 h treatment with the respective compound compared to untreated cells. * *p* < 0.05 (unpaired Student's *t*-test, always compared to untreated control). Displayed are the mean ± standard deviation values of at least six samples pooled from at least two biological replicates.

with the osmium complexes than 4T1 cells. In particular, the AV+/PI+ population increased significantly to 40.3% ([**1**]), 36.0% (Na[**1**]) and 57.2% ([**3**]) upon treatment (*vs.* 15.1% untreated, $p < 0.05$), indicating that the *trans*-isomer induced apoptosis most effectively in HT29 cells (Fig. 8b).

In the cisplatin sensitive 4T1 cells, we also observed a significant increase in the AV+/PI+ population for all osmium compounds, but it was less pronounced ([**1**]: 27.7%, Na[**1**]: 33.9%, *trans*-[$Os^{IV}Cl_4(\kappa N1\text{-}2H\text{-ind})_2$]: 27.6%, untreated: 16.8%) and the *cis*- and *trans*-isomers [**1**] and [**3**] showed no difference (Fig. 8b).

In addition to flow cytometry data, we also measured cell viability and cell number of each sample in an automated cell counter. We found more pronounced effects on cell count than on cell viability, indicating that proliferation was affected, but the cells remained viable (Fig. 8c). In HT29 cells, cell viability was significantly affected by cisplatin, Na[**1**] and [**3**]. The cell number was strongly reduced by over 75% by all osmium compounds and to 41% by cisplatin (Fig. 8c). In 4T1 cells, the strongest effect on cell count was observed for the *cis*-compound Na[**1**] (20.9% of untreated), followed by cisplatin at 39.5% (Fig. 8c).

Conclusion

In this work we reported on the synthesis and crystal structure of *cis*-[$Os^{IV}Cl_4(\kappa N2\text{-}1H\text{-ind})_2$] ([**1**]), the first *cis*-configured isomer in the series of compounds of the general formula [$Os^{IV}Cl_4(Hazole)_2$], where Hazole = indazole, pyrazole, benzimidazole, and imidazole. In addition, we showed that *trans*-[$Os^{IV}Cl_4(\kappa N2\text{-}1H\text{-ind})_2$] ([**2**]) is also available, although more effective synthetic routes still need to be developed. Both compounds are complementary to their elsewhere reported *trans*-isomer [$Os^{IV}Cl_4(\kappa N1\text{-}2H\text{-ind})_2$] ([**3**]). Electrochemical and chemical one-electron reduction of [**1**] afforded *cis*-configured osmium(III) species isolated as tetrabutylammonium and sodium salts, *n*Bu$_4$N[**1**] and Na[**1**], respectively. X-band EPR spectra of *n*Bu$_4$N[**1**] in Me$_2$SO at 94 K and Na[**1**] in H$_2$O/ethylene glycol 5 : 1 v/v at 12 K are characterized by ill-resolved broad lines with a rhombic *g*-tensor indicating the low-spin $5d^5$ ($S = \frac{1}{2}$) electronic configuration of osmium(III) in these complexes. A simple ligand-field theory analysis of the *g* values indicates that in these *cis*-isomers, the electronic configuration differs from that of *trans*-analogs in that the electron "hole" is primarily in a $d_{xz,yz}$ orbital as opposed to a d_{xy} orbital in the much more commonly found species with *trans*-geometry. The *g*-tensor of the Os^{III} complexes of interest was further probed by quantum chemical theory. Specifically, the *g*-tensor values calculated by DKS/COSMO theory (with involvement of the solvent model) are in quite good agreement with those determined experimentally. Access to both *cis*- and *trans*-isomers of osmium(IV) and osmium(III) that are water soluble prompted us to investigate their *in vitro* anti-cancer activities. The complexes [**1**], Na[**1**] and [**3**] showed antiproliferative effects on cancer cells which were not coupled to their sensitivity to cis-

platin. Cytostatic effects were stronger than actual cell killing at 48 h incubation time. HT29 cells showed a higher sensitivity to treatment with osmium complexes than cisplatin. 4T1 cells showed lower rates of apoptosis induction by the osmium complexes than cisplatin, but a very strong cytostatic effect was observed for the *cis*-isomer Na[**1**]. The unavailability of a larger scale procedure for the synthesis of the *trans*-isomer [**2**] makes the direct disclosure of the effect of geometrical isomerism on cytotoxicity in this case not possible. From the other side, a direct extrapolation of the results of the antiproliferative activity and cytostatic effects of the *cis*-isomer Na[**1**] on the ruthenium analogues is not possible as well, if one takes into account the body of accumulated evidence and cytotoxicity data for related ruthenium and osmium compounds[28,29,35,57,60,86–91] and complexity of the problem.[92] Even though the analogous *cis*-isomers of KP1019/NKP1339 remain unknown, their synthesis appears to be imminent, giving an opportunity that deserves to be exploited in the search for more effective metal-based anticancer drugs than those currently in clinical trials.

Conflicts of interest

The authors declare no competing financial interest.

Acknowledgements

References

1 C. J. Mathews, S. P. Barnett, S. C. Smith, N. J. Barnes, W. G. Whittingham, J. Williams, E. D. Clarke, A. J. Whittle, D. J. Hughes, S. Armstrong, R. Viner, T. E. Macleod Fraser, P. J. Crowley, R. Salmon and B. L. Pilkington, Pesticidal indazole or benzotriazole derivatives, *Internat. Patent WO* 2000/063207A1, 2000.

2 J. Hood, D. M. Wallace and S. Kumar, Indazole inhibitors of the wnt signal pathway and therapeutic uses thereof, *Internat. Patent WO* 2011/019651A1, 2011.

3 H. Cerecetto, A. Gerpe, M. González, V. J. Arán and C. Ochoa de Ocáriz, *Mini-Rev. Med. Chem.*, 2005, **5**, 869–878.

4 J. Elguero, I. Alkorta, R. M. Claramunt, C. Lopez, D. Sanz and D. Santa Maria, *Bioorg. Med. Chem.*, 2009, **17**, 8027–8031.

5 J. Zhang, Q. Yang, J. A. C. Romero, J. Cross, B. Wang, K. M. Poutsiaka, F. Epie, D. Bevan, Y. Wu, T. Moy, A. Daniel, B. Chamberlain, N. Carter, J. Shotwell, A. Arya, V. Kumar, J. Silverman, K. Nguyen, C. A. Metcalf, D. Ryan, B. Lippa and R. E. Dolle, *ACS Med. Chem. Lett.*, 2015, **6**, 1080–1085.

6 V. Sandanayaka, J. Singh, L. Zhao and M. E. Gurney, N-linked aryl heteroaryl inhibitors of lta4h for treating inflammation, *Patent US* 2007/0142434A1, 2007.

7 K. Down, A. Amour, I. R. Baldwin, A. W. J. Cooper, A. M. Deakin, L. M. Felton, S. B. Guntrip, C. Hardy, Z. A. Harrison, K. L. Jones, P. Jones, S. E. Keeling, J. Le, S. Livia, F. Lucas, C. J. Lunniss, N. J. Parr, E. Robinson, P. Rowland, S. Smith, D. A. Thomas, G. Vitulli, Y. Washio and J. N. Hamblin, *J. Med. Chem.*, 2015, **58**, 7381–7399.

8 D. Shaw, S. M. Wang, A. G. Villasenor, S. Tsing, D. Walter, M. F. Browner, J. Barnett and A. Kuglstatter, *J. Mol. Biol.*, 2008, **383**, 885–893.

9 K. Schiemann, A. Mallinger, D. Wienke, C. Esdar, O. Poeschke, M. Busch, F. Rohdich, S. A. Eccles, R. Scheider, F. I. Raynaud, P. Czodrowski, D. Musil, D. Schwarz, K. Urbahns and J. Blagg, *Bioorg. Med. Chem. Lett.*, 2016, **26**, 1443–1451.

10 (*a*) H. A. Burris, S. Bakewell, J. C. Bendell, J. Infante, S. F. Jones, D. R. Spigel, G. J. Weiss, R. K. Ramanathan, A. Ogden and D. von Hoff, *ESMO Open*, 2016, **1**, e000154; (*b*) interzyne.com/it-139/.

11 A. Schmidt, A. Beutler and B. Snovydovych, *Eur. J. Org. Chem.*, 2008, 4073–4095.

12 W. Stadlbauer, *Sci. Synth.*, 2002, **12**, 227–324.

13 M. J. Haddadin, W. E. Conrad and M. J. Kurth, *Mini-Rev. Med. Chem.*, 2012, **12**, 1293–1300.

14 P.-S. Kuhn, S. M. Meier, K. K. Jovanović, I. Sandler, L. Freitag, G. Novitchi, L. González, S. Radulović and V. B. Arion, *Eur. J. Inorg. Chem.*, 2016, 1566–1576.

15 G. E. Büchel, I. N. Stepanenko, M. Hejl, M. A. Jakupec, B. K. Keppler and V. B. Arion, *Inorg. Chem.*, 2011, **50**, 7690–7697.

16 G. E. Büchel, I. N. Stepanenko, M. Hejl, M. A. Jakupec, B. K. Keppler, P. Heffeter, W. Berger and V. B. Arion, *J. Inorg. Biochem.*, 2012, **113**, 47–54.

17 B. Rosenberg, L. Van Camp and T. Krigas, *Nature*, 1965, **205**, 698–699.

18 M. J. Cleare and J. D. Höschele, *Platinum Met. Rev.*, 1973, **17**, 2–13.

19 M. J. Cleare and J. D. Höschele, *Bioinorg. Chem.*, 1973, **2**, 187–210.

20 (*a*) N. Farrell, T. T. B. Ha, J. P. Souchard, F. L. Wimmer, S. Cros and N. P. Johnson, *J. Med. Chem.*, 1989, **32**, 2240–2241; (*b*) E. I. Montero, S. Diaz, A. M. Gonzalez-Vadillo, J. M. Perez, C. Alonso and C. Navarro-Ranninger, *J. Med. Chem.*, 1999, **42**, 4264–4268; (*c*) S. van Zutphen, E. Pantoja, R. Soriano, C. Soro, D. M. Tooke, A. L. Spek, H. Den Dulk, J. Brouwer and J. Reedijk, *Dalton Trans.*, 2006, 1020–1023; (*d*) S. Grabner, B. Modec, N. Bukovec, P. Bucovec, M. Čemažar, S. Kranjc, G. Serša and J. Sčančar, *J. Inorg. Biochem.*, 2016, **161**, 40–51.

21 (*a*) L. R. Kelland, C. F. J. Barnard, I. G. Evans, B. A. Murrer, B. R. C. Theobald, S. B. Wyer, P. M. Goddard, M. Jones, M. Valenti, A. Bryant, P. M. Rogers and K. R. Harrap, *J. Med. Chem.*, 1995, **38**, 3016–3024; (*b*) M. Coluccia, A. Nassi, A. Boccarelli, D. Giordano, N. Cardellicchio, D. Locker, M. Leng, M. Sivo, F. P. Intini and G. Natile, *J. Inorg. Biochem.*, 1999, **77**, 31–35.

22 (*a*) A. Werner, *Ber. Dtsch. Chem. Ges.*, 1908, **40**, 4817–4825; (*b*) A. Werner, *Z. Anorg. Chem.*, 1897, **14**, 28–41.

23 (*a*) V. B. Arion, E. Reisner, M. Fremuth, M. A. Jakupec, B. K. Keppler, V. Y. Kukushkin and A. J. L. Pombeiro, *Inorg. Chem.*, 2003, **42**, 6024–6031; (*b*) B. K. Keppler, K.-G. Lipponer, B. Stenzel and F. Kratz, New tumor-inhibiting ruthenium complexes, in *Metal Complexes in Cancer Chemotherapy*, ed. B. K. Keppler, VCH, 1993, pp. 187–220; (*c*) I. N. Stepanenko, B. Cebrian-Losantos, V. B. Arion, A. A. Krokhin, A. A. Nazarov and B. K. Keppler, *Eur. J. Inorg. Chem.*, 2007, 400–411.

24 W. X. Ni, W. L. Man, S. M. Yiu, M. Ho, M. T. W. Cheung, C. C. Ko, C. M. Che, Y. W. Lam and T. C. Lau, *Chem. Sci.*, 2012, **3**, 1582–1588.

25 A. M. Basri, R. M. Lord, S. J. Allison, A. Rodriguez-Barzano, S. J. Lucas, F. D. Janeway, H. J. Shepherd, C. M. Pask, R. M. Phillips and P. C. McGowan, *Chem. – Eur. J.*, 2017, **23**, 6341–6356.

26 S. Kolf and W. Preetz, *Z. Anorg. Allg. Chem.*, 1999, **625**, 411–416.

27 (*a*) A. Doadrio, D. Craciunescu, C. Ghirvu and J. C. Nuno, *An. Quim.*, 1977, **73**, 1220–1223; (*b*) S.-W. Lai, Q. K.-W. Chan, N. Zhu and C.-M. Che, *Inorg. Chem.*, 2007, **46**, 11003–11016; (*c*) I. Kostova and R. K. Soni, *Int. J. Curr. Chem.*, 2010, **1**, 133–143; (*d*) W.-X. Ni, W.-L. Man, M. T.-W. Cheung, R. W.-Y. Sun, Y.-L. Shu, Y.-W. Lam, C.-M. Che and T.-C. Lau, *Chem. Commun.*, 2011, **47**, 2140–2142; (*e*) Q. Tang, W.-X. Ni, C.-F. Leung, W.-L. Man, K. K.-K. Lau, Y. Liang, Y.-W. Lam, W.-Y. Wong, S.-M. Peng, G.-J. Liu and T.-C. Lau, *Chem. Commun.*, 2013, **49**, 9980–

9982; (*f*) W.-L. Man, W. W. Y. Lam and T.-C. Lau, *Acc. Chem. Res.*, 2014, **47**, 427–439; (*g*) K. Suntharalingam, W. Lin, T. C. Johnstone, P. M. Bruno, Y.-R. Zheng, M. T. Hemann and S. J. Lippard, *J. Am. Chem. Soc.*, 2014, **136**, 14413–14416; (*h*) S. A. E. Omar, P. A. Scattergood, L. K. McKenzie, H. E. Bryant, J. A. Weinstein and P. I. P. Elliott, *Molecules*, 2016, **21**, 1382, DOI: 10.3390/molecules21101382; (*i*) J. Zhu, A. Dominijianni, J. Á. Rodríguez-Corrales, R. Prussin, Z. Zhao, T. Li, J. L. Robertson and K. J. Brewer, *Inorg. Chim. Acta*, 2017, **454**, 155–161; (*j*) C. Yang, W. Wang, G.-D. Li, H.-J. Zhong, Z.-Z. Dong, C.-Y. Wong, D. W. J. Kwong, D.-L. Ma and C.-H. Leung, *Sci. Rep.*, 2017, **7**, 42860, DOI: 10.1038/srep42860.

28 I. N. Stepanenko, G. E. Büchel, B. K. Keppler and V. B. Arion, Osmium complexes with azole heterocycles as potential antitumor drugs, in *Encyclopedia of Metalloproteins*, ed. R. H. Kretsinger, V. N. Uversky and V. N. Permyakov, Springer, New York, 2013, pp. 1596–1614.

29 P.-S. Kuhn, G. E. Büchel, K. K. Jovanović, L. Filipović, S. Radulović, P. Rapta and V. B. Arion, *Inorg. Chem.*, 2014, **53**, 11130–11139.

30 B. Verdejo, L. Acosta-Rueda, P. M. Clares, A. Aguinaco, M. G. Basallote, C. Soriano, R. Tejero and E. García-España, *Inorg. Chem.*, 2015, **54**, 1983–1991.

31 K. E. Prosser and C. J. Walsby, *Eur. J. Inorg. Chem.*, 2017, 1573–1585.

32 M. L. Souza, E. E. Castellano, J. Telser and D. W. Franco, *Inorg. Chem.*, 2015, **54**, 2067–2080.

33 (*a*) P. H. Rieger, *Coord. Chem. Rev.*, 1994, **135/136**, 203–286; (*b*) B. R. McGarvey, *Coord. Chem. Rev.*, 1998, **170**, 75–92; (*c*) B. R. McGarvey, N. C. Batista, C. W. B. Bezerra, M. S. Schultz and D. W. Franco, *Inorg. Chem.*, 1998, **37**, 2865–2872.

34 S. Kremer, *Inorg. Chim. Acta*, 1984, **85**, 57–60.

35 I. N. Stepanenko, A. A. Krokhin, R. O. John, A. Roller, V. B. Arion, M. A. Jakupec and B. K. Keppler, *Inorg. Chem.*, 2008, **47**, 7338–7347.

36 S. Stoll and A. Schweiger, *J. Magn. Reson.*, 2006, **178**, 42–55.

37 *SAINT-Plus (Version 7.06a) and APEX2*, Bruker-Nonius AXS Inc., Madison, Wisconsin, USA, 2004.

38 G. M. Sheldrick, *Acta Crystallogr., Sect. A: Fundam. Crystallogr.*, 2008, **A64**, 112–122.

39 M. N. Burnett and G. K. Johnson, ORTEPIII. Report ORNL-6895, OAK Ridge National Laboratory, Oak Ridge, TN, 1996.

40 M. J. Frisch, G. W. Trucks, H. B. Schlegel, G. E. Scuseria, M. A. Robb, J. R. Cheeseman, G. Scalmani, V. Barone, B. Mennucci, G. A. Petersson, H. Nakatsuji, M. Caricato, X. Li, H. P. Hratchian, A. F. Izmaylov, J. Bloino, G. Zheng, J. L. Sonnenberg, M. Hada, M. Ehara, K. Toyota, R. Fukuda, J. Hasegawa, M. Ishida, T. Nakajima, Y. Honda, O. Kitao, H. Nakai, T. Vreven, J. A. Montgomery, Jr., J. E. Peralta, F. Ogliaro, M. Bearpark, J. J. Heyd, E. Brothers, K. N. Kudin, V. N. Staroverov, R. Kobayashi, J. Normand, K. Raghavachari, A. Rendell, J. C. Burant, S. S. Iyengar, J. Tomasi, M. Cossi, N. Rega, J. M. Millam, M. Klene,

J. E. Knox, J. B. Cross, V. Bakken, C. Adamo, J. Jaramillo, R. Gomperts, R. E. Stratmann, O. Yazyev, A. J. Austin, R. Cammi, C. Pomelli, J. W. Ochterski, R. L. Martin, K. Morokuma, V. G. Zakrzewski, G. A. Voth, P. Salvador, J. J. Dannenberg, S. Dapprich, A. D. Daniels, Ö. Farkas, J. B. Foresman, J. V. Ortiz, J. Cioslowski and D. J. Fox, *Gaussian 09, revision D.01*, Gaussian, Inc., Wallingford, CT, 2009.

41 (*a*) C. Lee, W. Yang and R. G. Parr, *Phys. Rev. B: Condens. Matter Mater. Phys.*, 1988, **37**, 785–789; (*b*) A. D. Becke, *J. Chem. Phys.*, 1993, **98**, 5648–5652; (*c*) P. J. Stephens, F. J. Devlin, C. F. Chabalowski and M. J. Frisch, *J. Phys. Chem.*, 1994, **98**, 11623–11627; (*d*) S. H. Vosko, L. Wilk and M. Nusair, *Can. J. Phys.*, 1980, **58**, 1200–1211.

42 (*a*) A. Schaefer, H. Horn and R. Ahlrichs, *J. Chem. Phys.*, 1992, **97**, 2571–2577; (*b*) F. Weigend and R. Ahlrichs, *Phys. Chem. Chem. Phys.*, 2005, **7**, 3297–3305.

43 D. Andrae, U. Häußermann, M. Dolg, H. Stoll and H. Preuß, *Theor. Chim. Acta*, 1990, **77**, 123–141.

44 (*a*) F. Neese and E. I. Solomon, *Inorg. Chem.*, 1998, **37**, 6568–6582; (*b*) F. Neese, *J. Chem. Phys.*, 2001, **115**, 11080–11096; (*c*) F. Neese, *Chem. Phys. Lett.*, 2003, **380**, 721–728; (*d*) F. Neese, *J. Chem. Phys.*, 2005, **122**, 034107; (*e*) F. Neese, *Mol. Phys.*, 2007, **105**, 2507–2514; (*f*) B. Sandhoefer and F. Neese, *J. Chem. Phys.*, 2012, **137**, 094102; (*g*) D. Ganyushin and F. Neese, *J. Chem. Phys.*, 2013, **138**, 104113; (*h*) M. Mader-Cosper, F. Neese, A. V. Astashkin, M. A. Carducci, A. M. Raitsimring and J. H. Enemark, *Inorg. Chem.*, 2005, **44**, 1290–1301.

45 F. Neese, The ORCA program system, *Wiley Interdiscip. Rev.: Comput. Mol. Sci.*, 2012, **2**, 73–78.

46 (*a*) E. van Lenthe, E. J. Baerends and J. G. Snijders, *J. Chem. Phys.*, 1993, **99**, 4597–4610; (*b*) C. van Wüllen, *J. Chem. Phys.*, 1998, **109**, 392–399.

47 (*a*) F. E. Jorge, A. Canal Neto, G. G. Camiletti and S. F. Machado, *J. Chem. Phys.*, 2009, **130**, 064108; (*b*) A. Canal Neto and F. E. Jorge, *Chem. Phys. Lett.*, 2013, **582**, 158–162.

48 S. Sinnecker, A. Rajendran, A. Klamt, M. Diedenhofen and F. Neese, *J. Phys. Chem. A*, 2006, **110**, 2235–2245.

49 S. Komorovsky, M. Repisky, V. G. Malkin, O. L. Malkina, M. Kaupp and K. Ruud, with contributions from R. Bast, U. Ekström, M. Kadek, S. Knecht, L. Konecny, E. Malkin, I. Malkin-Ondik, R. Di. Remigio, *ReSpect, version 3.5.0 2016 – Relativistic Spectroscopy DFT program of authors* http//www.respectprogram.org.

50 M. Repisky, S. Komorovsky, E. Malkin, O. L. Malkina and V. G. Malkin, *Chem. Phys. Lett.*, 2010, **488**, 94–97.

51 R. Di. Remigio, M. Repisky, S. Komorovsky, P. Hrobarik, L. Frediani and K. Ruud, *Mol. Phys.*, 2017, **115**, 214–227.

52 I. Malkin, O. L. Malkina, V. G. Malkin and M. Kaupp, *J. Chem. Phys.*, 2005, **123**, 244103.

53 P. Hrobarik, M. Repisky, S. Komorovsky, V. Hrobarikova and M. Kaupp, *Theor. Chem. Acc.*, 2011, **129**, 715–725.

54 S. Gohr, P. Hrobarik, M. Repisky, S. Komorovsky, K. Ruud and M. Kaupp, *J. Phys. Chem. A*, 2015, **119**, 12892–12905.

55 P. J. Cherry, S. Komorovsky, V. G. Malkin and O. L. Malkina, *Mol. Phys.*, 2016, **115**, 75–89.

56 J. A. Davies, C. M. Hockensmith, V. Yu. Kukushkin and Yu. N. Kukushkin, *Synthetic Coordination Chemistry – Principles and Practice*, World Scientific, Singapore, 1995, pp. 392–396.

57 G. E. Büchel, I. N. Stepanenko, M. Hejl, M. A. Jakupec, V. B. Arion and B. K. Keppler, *Inorg. Chem.*, 2009, **48**, 10737–10747.

58 I. Chiorescu, I. N. Stepanenko, V. B. Arion, A. A. Krokhin and B. K. Keppler, *J. Biol. Inorg. Chem.*, 2007, **12**(Suppl. 1), 226.

59 A. Gavriluta, G. E. Büchel, L. Freitag, G. Novitchi, J. B. Tommasino, E. Jeanneau, P.-S. Kuhn, L. González, V. B. Arion and D. Luneau, *Inorg. Chem.*, 2013, **52**, 6260–6272.

60 G. E. Büchel, A. Gavriluta, M. Novak, S. M. Meier, M. A. Jakupec, O. Cuzan, C. Turta, J.-B. Tommasino, E. Jeanneau, G. Novitchi, D. Luneau and V. B. Arion, *Inorg. Chem.*, 2013, **52**, 6273–6285.

61 (*a*) D. F. Rendle, A. Storr and J. Trotter, *Can. J. Chem.*, 1975, **53**, 2930–2943; (*b*) S. A. Cortes-Llamas, J. M. Hernández-Pérez, M. Hô and M.-A. Muñoz-Hernández, *Organometallics*, 2006, **25**, 588–595.

62 J. P. Fackler, Jr., R. J. Staples and R. G. Raptis, *Z. Kristallogr.*, 1997, **212**, 157–158.

63 W. Peti, T. Pieper, M. Sommer, B. K. Keppler and G. Giester, *Eur. J. Inorg. Chem.*, 1999, 1551–1555.

64 I. Bertini, C. Luchinat, G. Parigi and E. Ravero, *NMR of Paramagnetic Molecules, Volume 2, Second Edition: Applications to Metallobiomolecules and Models (Current Methods in Inorganic Chemistry)*, 2nd edn.

65 V. I. Azarov, A. J. J. Raassen, Y. N. Joshi, P. H. M. Uylings and A. N. Ryabtsev, *Phys. Scr.*, 1997, **56**, 325–343.

66 P. Roy, A. K. Jana, D. Das and D. N. Nath, *Chem. Phys. Lett.*, 2009, **474**, 297–301.

67 M. Mohsen-Nia, H. Amiri and B. Jazi, *J. Solution Chem.*, 2010, **39**, 701–708.

68 *Organic Solvents 3rd ed., Techniques of Organic Chemistry*, ed. J. A. Riddick and W. B. Bunger, Wiley-Interscience, New York, 1970, vol. 2.

69 J. Barthel, R. Bucher and B. Wurm, *J. Mol. Liq.*, 2002, **98–99**, 51–69.

70 S. E. McLain, A. K. Soper and A. Luzar, *J. Chem. Phys.*, 2006, **124**, 074502.

71 B. Cebrián-Losantos, E. Reisner, C. R. Kowol, A. Roller, S. Shova, V. B. Arion and B. K. Keppler, *Inorg. Chem.*, 2008, **47**, 6513–6523.

72 The Q-band EPR spectrum of Na[**1**] in H_2O/ethylene glycol (Fig. S10‡) corroborated the X-band spectrum, but the lines were even broader as a consequence of *g*-strain (field-dependent broadening effects) and only g_{max} was observable; the two lower *g* values being outside the magnetic field range.

73 J. Telser, EPR Interactions – Zero Field Splittings, in *eMagRes*, John Wiley & Sons, Ltd, 2017, p. 6, DOI: 10.1002/9780470034590.emrstm1501.

74 F. A. Walker, *Chem. Rev.*, 2004, **104**, 589–616.

75 An alternate basis set, which is analytically easier to handle, is that with a fictitious $l = 1$, where the d_{xy} orbital corresponds to $m_l = 0$ and the $d_{xz,yz}$ to linear combinations of $m_l = \pm 1$, so that the basis set is as follows:
$$|-1, \pm 1/2\rangle = d_{+1}{}^+ d_{+1}{}^- d_{xy}{}^+ d_{xy}{}^- d_{-1}{}^\pm;$$
$$|+1, \pm 1/2\rangle = d_{-1}{}^+ d_{-1}{}^- d_{xy}{}^+ d_{xy}{}^- d_{+1}{}^\pm;$$
$$|0, \pm 1/2\rangle = \pm i d_{+1}{}^+ d_{+1}{}^- d_{-1}{}^+ d_{-1}{}^- d_{xy}{}^\pm.$$

76 K. J. LaChance-Galang, P. Doan, M. J. Clarke, U. Rao, A. Yamano and B. M. Hoffman, *J. Am. Chem. Soc.*, 1995, **117**, 3529–3538.

77 M. J. Clarke, V. M. Bailey, P. E. Doan, C. D. Hiller, K. J. LaChance-Galang, H. Daghlian, S. Mandal, C. M. Bastos and D. Lang, *Inorg. Chem.*, 1996, **35**, 4896–4903.

78 Similar equations have been reported by many workers, going back to Griffith (J. S. Griffith, *The theory of transition metal ions*, Cambridge University Press, New York, 1961), but we prefer those by McGarvey for reasons explained in his works.[33b,c]

79 A. N. Ryabtsev, A. J. J. Raassen, W.-Ü. L. Tchang-Brillet, Y. N. Joshi, P. H. M. Uylings and V. I. Azarov, *Phys. Scr.*, 1998, **57**, 82–108.

80 Q. De Paula, A. A. Batista, O. R. Nascimento, A. J. Da Costa, M. S. Schultz, M. R. Bonfadini and G. Oliva, *J. Braz. Chem. Soc.*, 2000, **11**, 530–536.

81 (*a*) J. Telser, G. E. Büchel, I. N. Stepanenko and V. B. Arion, unpublished results; (*b*) M. I. Webb, R. A. Chard, Y. M. Al-Jobory, M. R. Jones, E. W. Y. Wong and C. J. Walsby, *Inorg. Chem.*, 2012, **51**, 954–956.

82 O. M. Ni Dhubhghaill, W. R. Hagen, B. K. Keppler, K.-G. Lipponer and P. J. Sadler, *J. Chem. Soc., Dalton Trans.*, 1994, 3305–3310.

83 P. Verma and J. Autschbach, *J. Chem. Theory Comput.*, 2013, **9**, 1052–1067.

84 F. Zobi, L. Kromer, B. Spingler and R. Alberto, *Inorg. Chem.*, 2009, **48**, 8965–8970.

85 G. C. Allen, R. Al-Mobarak, G. A. M. El-Sharkawy and K. D. Warren, *Inorg. Chem.*, 1972, **11**, 787–796.

86 B. C. E. Makhubela, M. Meyer and G. S. Smith, *J. Organomet. Chem.*, 2014, **772–773**, 229–241.

87 M. Hanif, M. V. Babak and C. G. Hartinger, *Drug Discovery Today*, 2014, **19**, 1640–1648.

88 B. Boff, C. Gaiddon and M. Pfeffer, *Inorg. Chem.*, 2013, **52**, 2705–2715.

89 A. F. A. Peacock, A. F. R. Habtemariam, V. Walland, F. P. A. Fabbiani, S. Parsons, R. E. Aird, D. I. Jodrell and P. J. Sadler, *J. Am. Chem. Soc.*, 2006, **128**, 1739–1748.

90 E. Paunescu, S. McArthur, M. Soudani, R. Scopelliti and P. J. Dyson, *Inorg. Chem.*, 2016, **55**, 1788–1808.

91 N. P. E. Barry, O. Zava, P. J. Dyson and B. Therrien, *J. Organomet. Chem.*, 2012, **705**, 1–6.

92 E. Alessio, *Eur. J. Inorg. Chem.*, 2017, 1549–1560.